# Performance Evaluation of Multihop Wireless in Local Loop Architectures

A Project Report

*submitted in partial fulfillment of the requirements*
*for the award of the degree of*

**Bachelor of Technology**

**in**

**Computer Science and Engineering**

*by*

Mythili Ranganath V.

*under the guidance of*

Prof. C. Siva Ram Murthy


DEPARTMENT OF COMPUTER SCIENCE AND ENGINEERING
INDIAN INSTITUTE OF TECHNOLOGY MADRAS
May 2004

# Certificate

This is to certify that the project entitled **Performance Evaluation of Multihop Wireless in Local Loop Architectures** submitted by **Mythili Ranganath V.** in partial fulfillment of the requirements for the award of the degree of **Bachelor of Technology**, is a bona-fide record of work carried out by her under my supervision and guidance at the Department of Computer Science and Engineering, Indian Institute of Technology, Madras.

Place: Chennai [Prof. C. Siva Ram Murthy]
Date:

# Acknowledgments

I am grateful to Prof. C. Siva Ram Murthy for giving me my first taste of research. I would also like to thank him for his guidance and encouragement during the course of my project.

I would like to thank Manoj for his invaluable inputs and Archana, Sriram, Dilip and Rohit for their company during the course of my project. I would also like to thank all the students at the HPCN Lab for providing a motivating work environment.

I would like to thank the faculty and staff of the Department of Computer Science and Engineering at IIT, Madras for making my undergraduate experience an intellectually stimulating one. In particular, I would like to thank the Head of the Department Prof. S. Raman and my faculty advisor Dr. Deepak Khemani for their guidance throughout my undergraduate study.

I would like to thank my branch mate Pratibha for her entertaining company during these four years. I would also like to thank my friends Madhuri and Kanu for all the wonderful times we have had together. My family has always been a constant source of strength in my life and no words can express my gratitude for them.

Place: Chennai [Mythili Ranganath V.]
Date:

# Abstract

The use of Wireless in Local Loop (WiLL) has generated considerable interest due to the advantages it offers such as ease and low cost of deployment and maintenance. With an increase in the number of subscribers in the network, it becomes expedient to employ spectrum reusability techniques such as the use of multihop relaying and directional antennas, in order to improve the capacity of the WiLL system. Throughput enhanced Wireless in Local Loop (TWiLL) is one such architecture that employs multihop relaying to reuse bandwidth. Directional multihop Wireless in Local Loop (DWiLL), a new architecture proposed in this work, employs a unique combination of directional multihop relaying in the uplink and single hop relaying in the downlink to improve the throughput of WiLL systems.

Analysis of the Call Acceptance Ratio (CAR) in TWiLL and DWiLL systems is non-trivial as the Erlang B formula no longer holds. In this report, we build multi-dimensional Markov Chains to analyze the performance of these systems. We also compare the results of our analysis with results from simulations. We observe that multihop relaying and directional antennas lead to a significant increase in the CAR of WiLL systems.

The free space propagation model that is normally used to model the radio channel is a very unrealistic model and does not consider the effects of reflection, diffraction, scattering, and multipath propagation that hinder transmissions in WiLL systems. In this report, we consider many realistic radio channel propagation models and study how they affect the performance of TWiLL and DWiLL systems through analysis and simulations.

# Table of Contents

# List of Figures

# List of Tables

# CHAPTER 1

# Introduction

With recent performance improvements in computer and wireless technologies, advanced mobile wireless communication is expected to encounter extensive use and application in the near future. The phenomenal growth of the Internet and wireless connectivity has caused an explosive need for higher capacity wireless networks which can efficiently handle a variety of network loads, service highly mobile users with smooth hand-offs, offer connectivity through a variety of access points, manage both best-effort and real-time connections concurrently with QoS support for delay sensitive applications and above all be extendible from the existing infrastructure to form the basis of the Fourth Generation (4G) cellular systems. While cellular systems are designed to serve mobile users, another arena in which wireless communication has made a mark is in the local loop which is the last hop in the connection between a fixed subscriber and the Public Switched Telephone Network (PSTN).

*A Wireless in Local Loop (WiLL)* system consists of a set of fixed subscribers connected to the PSTN through a radio link in the last hop [1]. The geographical region is divided into cells with a *Base Transceiver Station (BTS)* at the center of each cell. The BTS interfaces with the fixed subscribers over the wireless link and with the PSTN over a wired link. The equipment that resides at the subscriber premises which is used to communicate with the BTS is called a *Fixed Subscriber Unit (FSU)*. Several WiLL technologies such as Digital Enhanced Cordless Telecommunication (DECT) [2], Personal Access Communication System (PACS) [3], and Personal Handyphone System (PHS) [4] have been developed whose architectures directly depend on the stationary nature of subscribers.

In the recent past there has been a rather heavy proliferation of mobile subscribers. While the subscriber density increases, the electromagnetic spectrum's capacity remains the same thus limiting the number of subscribers who can be simultaneously served. This is the single biggest stumbling block faced by wireless network operators in expanding their network and improving their subscriber base thus boosting profits. Just as in cellular systems, this problem stalks WiLL systems also. This would be detrimental to WiLL in particular since WiLL systems though a cheaper alternative to the copper wired local loops, are expected to provide the same level of service as the latter. The electromagnetic spectrum being limited, throughput enhancement is mainly achieved through a more efficient use of the available bandwidth. The basic ingredient in most recent throughput enhancement attempts has been the introduction of Ad hoc network characteristics which enhance the bandwidth reuse. This is shown by the development of architectures such as Integrated Cellular and

Ad hoc Relaying system (iCAR) [5], [6], Hybrid Wireless Network (HWN) [7] and Multihop Cellular Network (MCN) [8], [9]. *Throughput enhanced Wireless in Local Loop (TWiLL)* [10] is one such architecture which utilizes methods like multihop relaying and shortcut relaying to reuse system bandwidth.

The main disadvantage of TWiLL is that it does not work with directional antennas. Since WiLL systems mainly operate in Wide Area Network (WAN) domain with fixed or limited mobility subscribers, it is very essential to support multihop relaying with directional antennas.

There have been suggestions [11], [12], and [13] towards the use of directional antennas in multihop radio networks. Ko *et al.* identified in [14], the inadequacy of the traditional Wireless LAN (WLAN) MAC protocols to work efficiently with the use of directional antennas. The omni directional MAC protocols waste the network resources by reserving over a larger region than what is necessary. The authors of [14] propose a new approach, Directional MAC (D-MAC), for using the directional capabilities for better bandwidth utilization. Their solution includes the use of either directional RTS (DRTS) and using both directional and omni directional RTS (ORTS). In essence, directional MAC schemes improve the network performance by allowing more number of simultaneous transmissions, when compared to traditional RTS-CTS exchanges. [15] is one of the few suggestions towards the use of directional antennas as an energy conserving strategy for Ad hoc wireless networks. The authors of [15] identify the energy savings that can be achieved with the use of directional antennas and proposed a four-step algorithm for synchronization which not only enables efficient communication, but also optimizes the total energy consumption and the network lifetime. The assumption made in [15] is that each node is equipped with a single directional antenna which is electronically steerable and can be pointed to any direction in the azimuth plane.

We propose in this report [27] a new high performance architecture for Wireless in Local Loop Systems - *Directional multihop Wireless in Local Loop (DWiLL)* that uses the dual throughput enhancement strategies of multihop relaying and the use of directional antennas, to not only reduce the energy expenditure at the FSUs but also provide enhanced throughput when the number of subscribers becomes large.

In this report, we also mathematically model the TWiLL and DWiLL architectures. In analyzing the performance of these multihop WiLL architectures, the traditional Erlang B Loss Formula can no longer be used to obtain the Call Acceptance Ratio (CAR). Hence, we use the concepts of multi dimensional Markov chains to analyze these systems. We have also simulated these architectures and verified our theoretical analysis by corroborating it with simulation results.

Another aspect of WiLL systems that we have considered is modeling the radio channel. The radio channel places fundamental limitations on the performance of wireless communication systems. The transmission path between the transmitter and receiver can vary from a simple line-of-sight path to one that is severely obstructed by buildings, mountains and foliage. Unlike wired channels that are predictable, radio channels are extremely random. Modeling the radio channel has been one of

the most difficult tasks in mobile radio design and is typically done in a statistical fashion. Propagation models have traditionally focused on predicting the average received signal strength at a given distance from the transmitter. The free space path loss model, which says that the received power varies inversely as the square of the distance from the transmitter, is insufficient in predicting received power in realistic situations. Hence more realistic propagation models have been proposed.

Propagation models that predict the mean signal strength for an arbitrary transmitter-receiver (T-R) separation distance are called *large scale propagation models* [16]. They are useful in estimating the radio coverage area of the transmitter. (The radio coverage area of the transmitter is the area around it where the received signal strength exceeds the carrier sensing threshold.) On the other hand, models which describe rapid fluctuations in the received signal strength over very short distances are called *small scale fading models*. Small scale fading is caused due to factors like mobility of the transmitter and/or receiver and due to superposition of the signals that arrive at the receiver through different paths (also referred to as multipath propagation). Rayleigh fading and Ricean fading are some of the popular fading models.

In Wireless in Local Loop systems, the transmitter and receiver antennas are typically mounted on roof tops and the FSUs can be assumed to have zero mobility. In such circumstances, we can ignore the effects of small scale fading. Thus we focus only on large scale propagation models in this report.

Large scale propagation models are mainly of two types: analytical and empirical. The empirical approach is based on fitting curves or analytical expressions that recreate a set of measured data. This has the advantage of implicitly taking into account all propagation factors, both known and unknown. However, the validity of an empirical model in environments different from those used to derive the model cannot be easily verified. The Log Distance model and the Log Normal model, described in Sections 3.5 and 3.6, are two simple empirical models. We have described both the analysis and simulation of these models applied to TWiLL and DWiLL systems. Har-Xia-Bertoni (HXB) model [17] is another such model.

On the other hand, analytical models identify the factors that impact the received power at the receiver and attempt to analytically predict the received power based on these factors. Reflection, diffraction and scattering are three basic propagation mechanisms which impact propagation in wireless communication environment. Reflection occurs when a propagating electromagnetic wave impinges upon an object which has very large dimensions when compared to the wavelength of the propagating wave. Diffraction occurs when the radio path between the transmitter and receiver is obstructed by a surface that has sharp irregularities or edges. Scattering occurs when the medium through which the wave travels consists of objects with dimensions that are small compared to the wavelength, and where the number of obstacles per unit volume is large. Section 3.7 describes the Walfisch Bertoni (WB) Model [18] which is a theoretical model that very closely models the WiLL environment that we are considering. Xia - Bertoni (XB) model [19], Vogler model [20], flat edge model [21] and slope diffraction model [22] are some other analytical models.

The rest of the report is organized as follows. Chapter 2 provides an overview of the TWiLL architecture and also introduces the new DWiLL architecture. Chapters 3 and 4 contain the details of the theoretical analysis and implementation of the TWiLL and DWiLL architectures respectively. Chapter 5 concludes the report and provides pointers to future work related to the topics discussed.

# CHAPTER 2

# The TWiLL and DWiLL Architectures

In this chapter, we provide a comprehensive description of the TWiLL and DWiLL architectures. We also explain the routing and call setup procedures in these architectures.

## 2.1 The TWiLL Architecture

The Throughput enhanced Wireless in Local Loop (TWiLL) architecture proposed in [10] is a multihop architecture for limited mobility systems such as Wireless in Local Loop (WiLL) which can be used in high density traffic environments.

The bandwidth available is split into one control channel and several data channels which are not clustered between cells. TWiLL solves the problem of network partitions by allotting a channel in single-hop mode, when there is no multi-hop path to the BTS. That is, in TWiLL, every channel is designated as a multi-hop channel (MC) or a single-hop channel (SC) as illustrated in Figure 2.1 (a). A node (a fixed subscriber unit in a Wireless in Local Loop system) transmits in the control channel, SCs with a range of $R$ (cell radius), and in the MCs with a range of $r = R/2$ thus keeping the reuse factor 2 among the MCs. The call establishment process is similar to that in Multihop Cellular Networks [8]. To establish a call a node sends a Route Request (*RReq*) packet to the BTS over the control channel. The BTS computes a multi-hop path and allocates MCs along the path from the node to itself using the same method as in MCN. If such a path cannot be obtained, then the node is given an SC to communicate directly with the BTS. The allocation of channels in single-hop mode reduces the spatial reuse of bandwidth thus reducing the network throughput, but will also increase the number of accepted calls when the node density is less, thus increasing the network throughput. The TWiLL architecture is illustrated in Figure 2.1. Nodes A and C are connected to the BTS through multi-hop paths. Node C can reach the BTS over 1 hop while A does so over 2 hops. Node B is in a partition and cannot reach the BTS through a multi-hop path. Hence it is allowed to use an SC to communicate with the BTS in single-hop mode.

The probability that a call's destination is within the same cell as the call's source is defined as the *locality* ($L$) of the system. In TWiLL, locality of traffic is used to improve the throughput by a technique called *shortcut relaying*. Figure 2.1 (b) describes shortcut relaying used in TWiLL. Node A sets up a call to node E which is present in the same cell. Under a normal WiLL-like call setup, a path would be

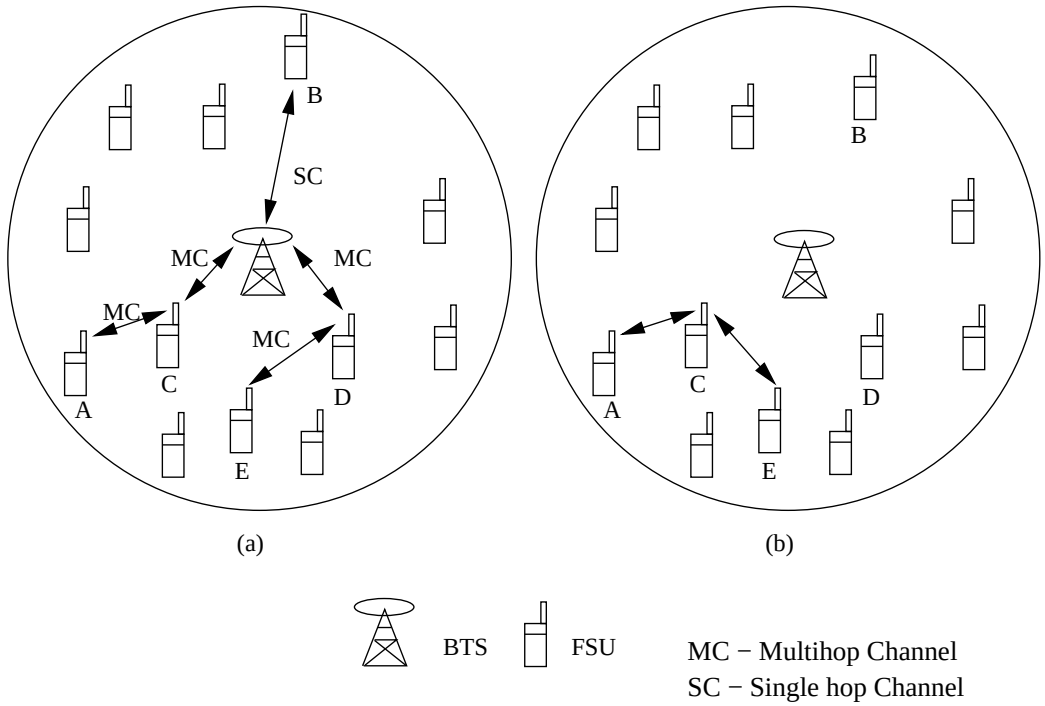


Figure 2.1: Multihop relaying in TWiLL (a) Normal Relaying (b) Shortcut Relaying

setup between node A and the BTS and another would be setup between BTS and node E as shown in Figure 2.1 (a). However this would not be very efficient since, node A might be able to reach node E without going through the BTS. This is shown in Figure 2.1 (b) where node A sets up a two hop path to node E. This path setup is coordinated by the BTS since node A does not have knowledge of the network topology. When such a path is computed, the BTS is also assumed as a relaying node and thus a path through the BTS may also be selected if it is the optimal one.

Since in TWiLL, users are mostly stationary or have very limited mobility, the number of path-reconfigurations will be much lesser than in MCN thus improving the quality of service. The stationary nature of subscribers also enables the use of directional antennas at the nodes, thus reducing the interference incurred at nodes in TWiLL.

## 2.2 The DWiLL Architecture

Directional multihop Wireless in Local Loop (DWiLL) is a new architecture that incorporates the additional feature of directional antennas at the nodes. It uses a unique combination of directional multihop relaying to improve throughput and single hop relaying to avoid network partitioning.

The use of directional antennas presents a useful technique for energy efficient

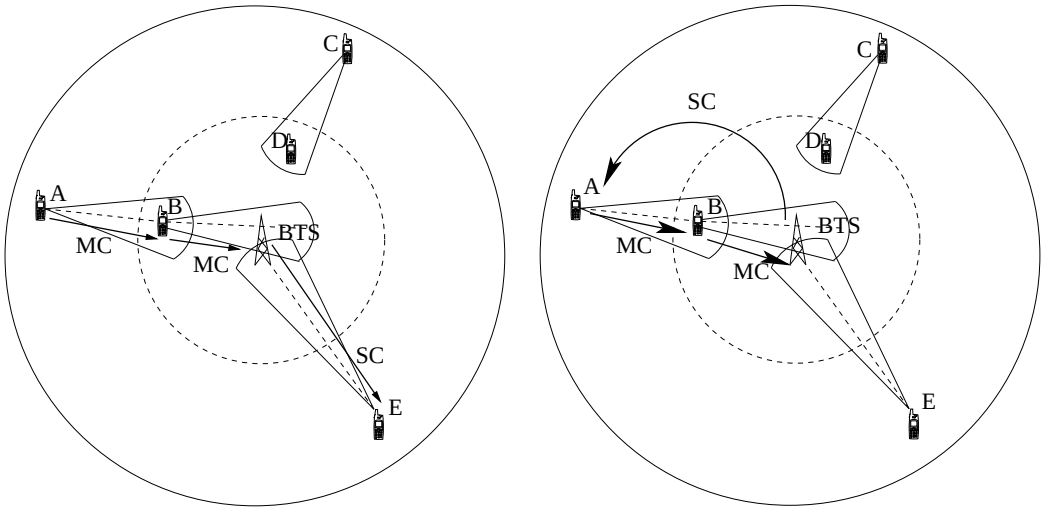


Figure 2.2: Illustration of call setup in DWiLL

transmission and throughput enhancement in Ad hoc wireless networks. Directional antennas also provide added advantages such as reduced probability of detection (crucial to military applications), lesser influence of hidden and exposed terminals, and lesser interference which leads to increased network throughput.

Data channels in DWiLL are divided into two categories *viz.,* Multihop Channels (MCs) and Single hop Channels (SCs). The SCs are further divided into Uplink Channels (ULCs) and Downlink Channels (DLCs). MCs operate over a transmission range of $r$ meters where $r$ is a fraction of the cell radius $R$ ($r = \frac{R}{k}$ where $k = 2$). The SCs operate over transmission range of $R$ meters. ULCs are assigned to those nodes that do not find intermediate relaying station to use MCs, in order to set up a data path to the BTS. The DLCs are used by the BTSs for the downlink transmissions to the FSUs. Figure 2.2 shows the call setup process in DWiLL. Figure 2.2 (a) shows a unidirectional call from FSU A to FSU E where a combination of directional multihop relaying in the uplink from FSU A to the BTS and single hop relaying in the downlink from the BTS to FSU E is used. Another case is shown in Figures 2.2 (b) where a duplex path is set up between FSU A to FSU B. On the unidirectional path $A \rightarrow B$, a single MC is allotted and the unidirectional path $B \rightarrow A$ is obtained through $B \rightarrow BTS \rightarrow A$ (an MC channel is assigned between FSU B and BTS and a DLC is assigned between BTS and FSU A). This technique of establishing a call directly between the source and destination nodes without the intervention of the BTS is called shortcut relaying, as in TWiLL. Shortcut relaying can be used to improve the throughput in systems with traffic locality.

Figures 2.3 (a)–(d) illustrate the advantages of DWiLL compared to the traditional single hop directional WiLL systems. Figure 2.3 (a) shows the channel alloca-

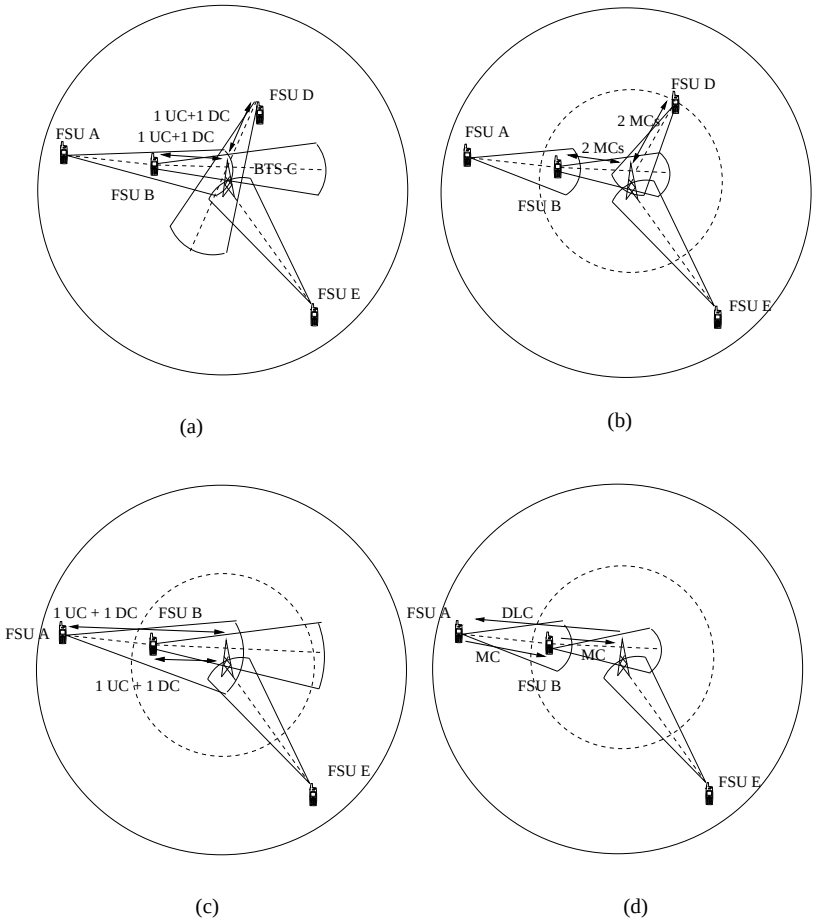


Figure 2.3: A comparison with traditional WiLL systems

tion between FSUs B and D in a given cell. It requires two (1 uplink channel and 1 down link channel) for the $B \rightarrow BTS$ and another two channels for the $BTS \rightarrow D$ link. These 4 channels cannot be reused in the cell. In such a scenario, DWiLL can complete the call with 4 MC channels as shown in Figure 2.3 (b). The advantage of DWiLL system is that these MC channels operate over a shorter transmission range making it reusable in the same cell. Figure 2.3 (c) shows another situation in traditional WiLL system, where the call between FSUs A and B requires 4 channels for duplex communication. For the same situation, DWiLL requires only 3 channels. One MC channel for the unidirectional link $A \rightarrow B$ and one MC channel and one DLC channel for the $B \rightarrow A$ unidirectional path obtained through $B \rightarrow BTS \rightarrow A$. Even in this case, the two MC channels used can be further reused. Hence the use of multihop relaying and directional antennas can enhance the capacity of the WiLL systems.

The system architecture in DWiLL is similar to the TWiLL [10], where the spectrum is divided into a number of channels. The key difference is the use of directional

relaying by the FSUs. We assume that the directionality is determined by the relative position of the FSU and the BTS. The directional antenna at the FSU needs to be oriented in the direction of the BTS. Since there is not a significant requirement for the directionality to be changed, there is no need for a sophisticated electronically and dynamically steerable antenna. The FSU will use the directional antenna to transmit control information, beacon signals, and the data messages. In our architecture we consider the directionality only in the azimuth plane, but the extension to directional relaying in both the azimuth and elevation should not be very different. We also note that due to the directionality, the wireless link level connectivity between two nodes is not symmetric.

The system works by building the topology information at the BTS as in [9]. All nodes, including the BTSs, send a *Beacon* to each other at regular intervals. Each node will report the set of nodes from which it receives the *Beacon*, along with the received power to the BTS. In addition to this, we have also modeled the interference that could result from the wireless transmission in two dimensions, radial and directional. We assume that the *Beacon* will be received with a certain power high enough to cause interference at nodes that are within the directional sector of radius $r \times (1 + \beta)$ and angle $\theta(1 + \gamma)$, where $r$ is the multihop transmission range (equal to half the cell radius), and $\theta$ is the azimuth of the directional antenna (the angular extent of transmission measured with respect to the radial line from the BTS to the FSU), and $\beta$ and $\gamma$ are the interference parameters (typically any directional transmission builds up primary and secondary lobes, which are modeled using a simple interference model for the channel allocation purpose) as illustrated in Figure 2.4.

The BTS builds up two topology matrices, the Multihop Connectivity Graph (MCG) $g$, the Single hop Connectivity Graph (SCG) $G$. The BTS also builds the interference matrices *R- Interference Matrix* and the *r-Interference Matrix*. The interference matrices refer to the channels at every node with significant level of interference such that the channel cannot be used at that node. The $R-InterferenceMatrix$ is associated with the single hop channel interference and the $r-InterferenceMatrix$ handles the same for the multihop channels. The *Interference Matrices* will contain all the channels used in the corresponding Connectivity Graphs (MCG and SCG) and the channels that receive interference from fringe transmitters as discussed earlier. For an omni directional antenna system the *Incidence Matrix* can be assumed to be symmetric, but this is not the case in the DWiLL architecture.

The signal receivable regions of the multihop channel is assumed to be a distance of $r$ meters in the direction of the receiver node and at an angle $\theta$ from the center line. The electromagnetic interference region is assumed to be extended to a distance of $r(1 + \alpha)$ radially and at an angular deviation of $\theta(1 + \beta)$ as shown in Figure 2.4. Any channel that is free of interference in this interference region is considered usable at any link in that region.

Routing in DWiLL is different from WiLL systems as it involves multihop relaying. Whenever a source node needs to setup a call session with another node, it requests the BTS by sending a *Route Request* packet over the control channel. The

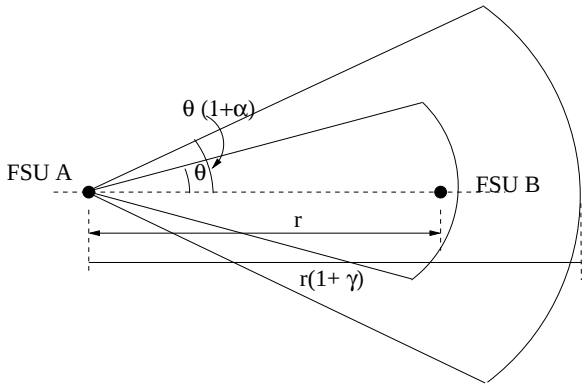


Figure 2.4: The interference regions

BTS in turn uses the shortest path algorithm to obtain a path to destination node (this path may include the BTS), and reserves the necessary channels at every intermediate link and replies with a *Route Reply* packet to the sender node. The route is obtained by a simple shortest path computation by the BTS using an appropriate metric. For a simplistic system we have assumed the hop-count metric for the path selection, but as suggested in [9] the enhanced edge weight (where the edge weight represents the number of nodes affected by the transmission) or similar metrics may also be used. Any given channel in the system can operate in four distinct modes: multihop, multihop-directional, single hop, and single hop-directional. The pure multihop (range= half the cell radius) and single hop (range=cell radius) transmission modes are used by the BTS to transmit the call. As the single hop and multihop channels are disjoint sets, the transmissions are mutually non-interfering. The FSUs can operate in either with transmission range equal to the cell-radius and directionality $\theta$ (single hop-directional), or with transmission range equal to half the cell radius and directionality $\theta$ (multihop-directional).

In the case when shortcut relaying is not used as in Figure 2.2(a), four sub calls have to be established during call setup. They are: (1) Source Uplink - The sub call from the source node to the BTS (2) Source Downlink - The sub call from the BTS to the source node (3) Destination Uplink - The sub call from the destination node to the destination BTS (4) Destination Downlink - The sub call from the destination BTS to the destination node. Each of these calls is setup using either SCs or MCs. The BTS successively tries these four calls and reserves channels. If the call setup fails due to unavailability of channels at any stage, the call is blocked and the resources reserved for that call upto that point are freed. A call is accepted only when channels are reserved for all four sub calls.

In the case when a multihop path exists between the source and destination, as in Figure 2.2(b), shortcut relaying technique is used. In this case, the source uplink call is directly setup between the source and destination nodes. Since call setup in DWiLL is asymmetric due to directionality, the destination connects to the source

through the BTS. Thus the destination uplink and source downlink calls are also setup in addition to the source uplink call.

# CHAPTER 3

# Performance Analysis of the TWiLL Architecture

In the previous chapter, we have studied two multihop WiLL architectures. We now theoretically analyse the performance of these architectures and prove that multihopping indeed improves the performance in WiLL systems. We choose Call Acceptance Ratio (CAR) - the ratio of the number of calls successfully connected to the number of calls tried - as the performance measure.

In this chapter, we theoretically derive the call acceptance ratio of a TWiLL system. In the first section, we analyze a simple TWiLL system where all calls originate and terminate in the same cell and where shortcut relaying is not used. We introduce traffic locality and shortcut relaying into the analysis in subsequent sections. We then incorporate some realistic propagation models into our analysis and simulations and observe their effects on the call accepting probability.

## 3.1 Analysis of a Simple TWiLL System

We now derive a mathematical expression for the call accepting probability of a simple TWiLL system without traffic locality and shortcut relaying. The simple free space propagation model is used in this section. Analysis for systems with traffic locality and shortcut relaying and systems with more realistic propagation models will be provided in the subsequent sections. The system under consideration has a certain fixed number of channels. Out of them, $m$ channels are used for multihop transmission (with a smaller radius $r$, typically equal to half the radius of the cell) and the remaining $S$ channels are used for single hop transmissions (that is, transmissions at radius equal to the radius of the cell $R$). The multihop channels can be further reused within a cell since a multihop transmission does not block the entire cell. Let $M$ denote the effective number of multihop channels available. There are $N$ nodes making calls in the cell. The combined call arrival rate is Poisson with mean $\nu$ and the holding time of each call is exponential with mean $\frac{1}{\mu}$. The traffic $T$ in the cell can be given as $\frac{\nu}{\mu}$ Erlang. We find the probability of acceptance of a call in such a system.

We recall that for a call originating and terminating in the same cell to be successful, four subcalls have to be established. They are: (1) Source Uplink - The subcall from the source node to the BTS (2) Source Downlink - The subcall from the BTS

to the source node (3) Destination Uplink - The subcall from the destination node to the destination BTS (4) Destination Downlink - The subcall from the destination BTS to the destination node.

### 3.1.1 Identification of various regions within a cell

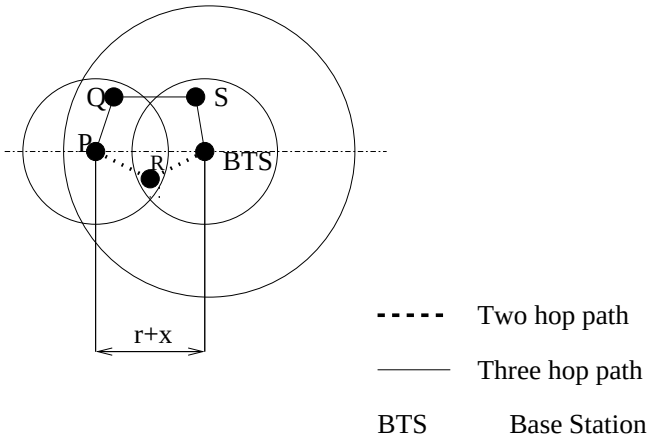


Figure 3.1: Two hop and three hop paths from a node to the BTS

To find the number of channels needed per call, we observe that the number of multihop and single hop channels needed depends upon the position of the source and destination nodes. We thus identify the various regions within a cell within which nodes require the same number of channels for call establishment. In other words, the hop length of the path between the node and the BTS is same for all nodes within a region and thus all nodes within a region will require the same number of multihop and single hop channels to establish a call.

We have identified four possible regions within a cell. (Note that the identification of regions is not made based not on any geographical criterion but purely on the hop length of the path between the node and the cell. Thus the word 'region' need not imply geographical contiguity.) Region 1: The node is within the inner subcell of radius $r$ and thus can reach the BTS using one multihop channel. Region 2: A two hop path exists from the node to the BTS. Region 3: A three hop path exists from the node to the BTS. Region 4: No multihop path exists from the source to the BTS. So the node connects to the BTS via a single hop channel. We have assumed that a single hop channel is used only when a multihop path does not exist. A single hop channel is not tried when a multihop path exists but multihop channel allocation fails. This assumption is justified because, for the kind of node densities that typically exist, a multihop path to the BTS exists with a high probability. Single hop channels are used when a node gets isolated from the other nodes (this is called a *partition*) and thus cannot use any multihop channels.

Note that, when the node density is sufficiently high, paths of hop length greater than $\frac{R}{r} + 1$ are formed with a very low probability. Hence we do not consider four and higher hop paths in our analysis. However, if the ratio $\frac{R}{r}$ increases, we need to consider paths of higher hop lengths also.

Let $PR(i)$ denote the probability that a node is in region $i$. Let $PR(i, j)$ denote the probability that the source is in region $i$ and destination is in region $j$ or vice versa. Obviously,

$$PR(i,j) = \begin{cases} PR(i) \times PR(j) & \text{if } i = j \\ 2 \times PR(i) \times PR(j) & \text{if } i \neq j \end{cases} \tag{3.1}$$

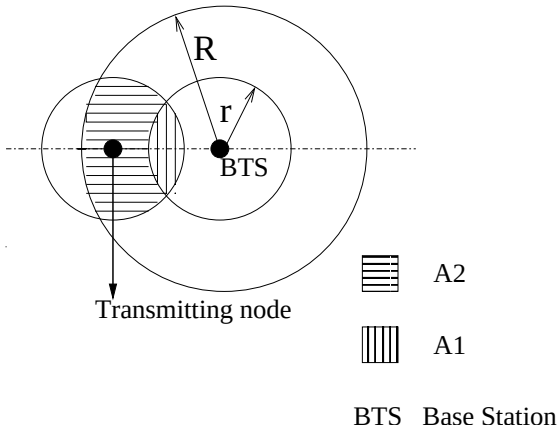


Figure 3.2: Calculating the probabilities that two hop and three hop paths exist from a node to the BTS

We now calculate the probabilities that a node is the various possible regions of a cell. A node is in the above described region 1 if it is within the inner subcell of radius $r$. Thus,

$$PR(1) = (\frac{r}{R})^2 \tag{3.2}$$

We now calculate the probability that a two hop path exists between a node and the BTS. In Figure 3.1, P - R - BTS is a two hop path to the BTS. This requires that the node is outside the subcell of radius $r$ and an intermediate node is found within the shaded region A1 shown in Figure 3.2. Probability that a node is at a distance $r+x$ from the center of the circle (for $x$ varying from 0 to $R-r$ ) is given by $\frac{2\pi(r+x)dx}{\pi R^2}$. Consider one such node that is at a distance of $r + x$ from the center of the cell. The inner subcell of the cell and the circle of radius $r$ around the cell (in which the node can potentially transmit) form two intersecting circles, as in Figure 3.2. Let the area of intersection be $A_1(x)$. (Refer Figure 3.2 shown above).

$$A_1(x) = r^2(q - \sin q) \text{ where } q = 2cos^{-1}(\frac{r+x}{2r}) \tag{3.3}$$

Now, for a multihop path to be found we require that atleast one node exists in this area to connect to the BTS. For any node, probability that it will not exist in this area is equal to $1 - \frac{A_1}{\pi R^2}$. Thus the probability that atleast one node exists in this area is given by $1 - (1 - \frac{A_1(x)}{\pi R^2})^{N-1}$. Thus, probability that a two hop path exists from a node to the BTS is given by,

$$PR(2) = \int_0^{R-r} \frac{2\pi(r+x)dx}{\pi R^2}(1 - (1 - \frac{A_1(x)}{\pi R^2})^{N-1}) \tag{3.4}$$

We now calculate the probability that a three hop path exists between a node and the BTS. A three hop path exists for a node P when another node Q exists in the region A2 (shown in Figure 3.2) and a two hop path to the BTS exists for Q through S (as shown in Figure 3.1). Let the node P be at a distance $r + x$ from the center of the cell. Then the required area in which node Q should be found is given by,

$$A_2(x) = Area(r, 2r, r + x) - A_1(x) \tag{3.5}$$

where $Area(r_1, r_2, d)$ denotes the area of overlap of two circles of radius $r_1$ and $r_2$ whose centers are distance $d$ apart. It is given by the formula

$$Area(r_1, r_2, d) = \frac{1}{2}r_1^2(t_1 - \sin t_1) + \frac{1}{2}r_2^2(t_2 - \sin t_2) \tag{3.6}$$

where

$$t_1 = 2cos^{-1}(\frac{r_1^2 + d^2 - r_2^2}{2r_1 d}) \tag{3.7}$$

and

$$t_2 = 2cos^{-1}(\frac{r_2^2 + d^2 - r_1^2}{2r_2 d}) \tag{3.8}$$

Probability that atleast one node exists in this area $A_2(x)$ is given by $1 - (1 - \frac{A_2(x)}{\pi R^2})^{N-1}$. A three hop path is taken when a two hop path is not available, an intermediate node exists and the intermediate node has a two hop path to the BTS. Thus, the probability that a three hop path exists from a node to the BTS is obtained by integrating over all possible values of $x$, as below.

$$PR(3) = \int_0^{R-r} [\frac{2\pi(r+x)dx}{\pi R^2}(1 - (1 - \frac{A_2(x)}{\pi R^2})^{N-1})] \times PR(2) \tag{3.9}$$

A single hop channel is used only when a multihop path does not exist. Thus, probability that a node uses a single hop channel to connect to the BTS is given by,

$$PR(4) = 1 - PR(1) - PR(2) - PR(3) \tag{3.10}$$

Table 3.1: Number of Channels Required to Establish a Call in a TWiLL System

| Region | $Rq_m$ | $Rq_s$ |
|---|---|---|
| 1 | 2 | 0 |
| 2 | 4 | 0 |
| 3 | 6 | 0 |
| 4 | 0 | 2 |

### 3.1.2 Number of channels required for the establishment of a call

We now estimate the number of channels needed for each location of the source and destination. Let $Rq_m(k)$ and $Rq_s(k)$ be the number of multihop and single hop channels needed to establish the source uplink and downlink calls when the source node is in position $k$. The values of $Rq_m(k)$ and $Rq_s(k)$ for all values of $k$ are given in Table 3.1.

Let $Rq_m(k,l)$ and $Rq_s(k,l)$ be the number of multihop and single hop channels required for both uplink and downlink calls for the source and destination when the source and destination nodes are in positions $k$ and $l$ or $l$ and $k$. Obviously, $Rq_m(k,l)$ is equal to $Rq_m(k) + Rq_m(l)$. Similarly for $Rq_s(k,l)$.

### 3.1.3 Computing the effective number of multihop channels

Since multihop channels are reused within a cell, the effective number of multihop channels $M$ is different from the actual number of multihop channels $m$ in a cell. We now compute the effective number of multihop channels available. Consider a

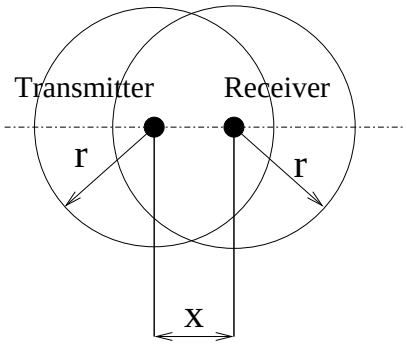


Figure 3.3: Area blocked by a multihop transmission

multihop transmission at a radius $r$ which is half the cell radius. Assume that the receiver is at a distance $x$ ($0 < x \leq r$). The channel used for this transmission cannot be reused in a circle of radius $r$ around the transmitter and the receiver. Let us denote the area blocked by a multihop transmission over a distance $x$ as $Blk(x)$. It

is given by the expression $\pi r^2 + \pi r^2 - r^2(q - sin(q))$ where $q = 2cos^{-1}\frac{x}{2r}$. This area blocked is as shown in the Figure 3.3. Let $Blk$ denote the average value of this area. It is given by

$$Blk = \int_0^r (\frac{2\pi x dx}{\pi r^2}) Blk(x) \tag{3.11}$$

Thus a multihop channel can be reused $\frac{\pi R^2}{Blk}$ number of times within a cell. Thus the effective number of multihop channels in a cell is given by

$$M = m \times \frac{\pi R^2}{Blk} \tag{3.12}$$

Note that, *this is an approximate theoretical upper limit of channel reuse.* The reuse is affected by the position in the cell where the multihop channel is used. Thus, by scaling the number of multihop channels as above, we will be overestimating the number of multihop channels available and thus the call acceptance probability values obtained from analysis will serve as an upper bound to the actual call acceptance probability values.

### 3.1.4 The formula for Call Acceptance Ratio

Let $Free_m(c)$ denote the probability that $c$ multihop channels are free in the system. Similarly, let $Free_s(c)$ denote the probability that $c$ single hop channels are free. Let $Free(c_m, c_s)$ denote the probability that $c_m$ multihop channels are $c_s$ single hop channels are free.

A call is accepted when the required number of channels are available to establish a call for a given location of source and destination. The expression for Call Acceptance Ratio (CAR) is thus given as

$$CAR = \sum_k \sum_l PR(k,l) Free(Rq_m(k,l), Rq_s(k,l)) \tag{3.13}$$

Hence, we need to find the variable $Free$ in the above equation, i.e., the probability that atleast $i$ multihop channels and $j$ single hop channels are available for any valid value of $i$ and $j$. To obtain this, it is enough of we know the probability that $i$ multihop channels and $j$ single hop channels are busy in the network at steady state for all values of $i$ and $j$. Let this probability be called $Busy(i,j)$.
In a communication system with $c$ channels and a traffic of $T$ Erlang, the probability that $k$ of the $c$ channels are occupied is given by the *Erlang B Loss Formula.*

$$B(k,T) = \frac{\frac{T^k}{k!}}{\sum_{i=1}^{c} \frac{T^i}{i!}} \tag{3.14}$$

The call blocking probability of such a system is the probability that all the $c$ channels are occupied at a given instant, and thus it is given by $B(c,T)$. Hence the call accepting probability is $1 - B(c,T)$.

But the Erlang B formula cannot be applied directly in our case because we have a system with two types of channels. Also the inflow of traffic to the two types of channels is not uniform. Thus, this formula cannot be used in our case. Hence, we adopt a different strategy of using the concept of a multi-dimensional Markov chains.

### 3.1.5 Building multi-dimensional Markov chains

A Markov chain is defined as a stochastic process which exists in one of the many possible states. The state of a Markov process is a random variable. A Markov chain is characterized by the fact that the probability of transition from one state to the other is independent of the process history prior to arriving at that state. Thus the probability of transition from state $i$ to $j$ is fixed and does not depend on the path by which the process arrived to state $i$. The matrix containing the transition probabilities from every state $i$ to every other state $j$ is called the transition probability matrix.

For an aperiodic, irreducible Markov chain which has a steady state distribution, the steady state probabilities are calculated by writing global balance equations [23]. Let $p_i$ be the steady state probability of the system being in state $i$. Let $P_{ij}$ be the probability of transition from state $i$ to $j$. Then, we have

$$\sum_i p_i P_{ij} = p_j \tag{3.15}$$

for all values of $j$. Let $p$ be the row vector of the steady state probabilities. Let $T$ be the transition probability matrix. Expressing the above equation in matrix form, we have,

$$pT = p \tag{3.16}$$

We model our system as a multi dimensional Markov chain - a Markov chain where the state is determined by more than one random variable. The system is said to be in state $(i, j)$ if $i$ out of the $M$ multihop channels and $j$ out of the $S$ single hop channels are being used. Let $Busy(i, j)$ be the steady state probability that the Markov process is in state $(i, j)$, i.e., the probability that $i$ multihop channels and $j$ single hop channels are occupied in steady state. Let the transition probability matrix be denoted by $Tr$. That is, the probability of transition from state $(i_1, j_1)$ to $(i_2, j_2)$ is given by the element $Tr((i_1, j_1), (i_2, j_2))$ for all possible pairs of states $(i_1, j_1)$ and $(i_2, j_2)$.

Let $Busy$ be the row vector containing the steady state probabilities $Busy(i, j)$ for all values of $i$ and $j$. We have the following equations

$$Busy \times Tr = Busy \tag{3.17}$$

$$\sum_i \sum_j Busy(i, j) = 1 \tag{3.18}$$

Note that $Busy$ is an $(M + 1)(S + 1)$ dimension row vector and $Tr$ is an $(M + 1)(S + 1) \times (M + 1)(S + 1)$ matrix.

From Equations 3.17 and 3.18, the probabilities $Busy(i,j)$ can be found for all values of $i$ and $j$ if we know the matrix $Tr$. So all that remains to be computed is the transition probability matrix. The next section is devoted to this issue.

### 3.1.6 Computing transition probabilities

In this section, we generate the entries of the transition probability matrix in a systematic manner. As observed earlier, the CAR can be obtained easily once the transition probability matrix is filled.

Let all the users of the system have a combined call generating rate of $\nu$. The arrival of calls is assumed to be Poisson with mean $\nu$ and the service time (*i.e.*, the holding time) of calls is assumed to be exponential with mean $\frac{1}{\mu}$. Assume that the system is in a steady state. Consider an infinitesimally small interval of time $dt$. The interval is small enough to assume that only one event (either a call arrival or a call departure) can occur in that time. Also assume that system is in state $(i,j)$ at time $t$. The state of the system at time $t+dt$ depends on whether a call has arrived or departed in the interval.

We assume that the arrival rate of the system $\nu$ is independent of the state of the system. Thus $\nu(i,j)$ is equal to $\nu$ for all $i$ and $j$. Thus the probability that a call arrives in the interval $dt$ is given by $\nu dt$.

Let the service rate of the system in state $(i,j)$ be $\mu(i,j)$. The service rate of one call of the system is $\mu$. Let the number of active calls of the system be $C$. Then the service rate of the system is given by

$$\mu(i,j) = C\mu \tag{3.19}$$

The value of $C$ cannot be uniquely determined from the state of the system. Thus we use an approximate method to find $C$. Let $AvgCh$ denote the average number of channels (either multihop or single hop) used per call. We have

$$AvgCh = \sum_k \sum_l PR(k,l)[Rq_m(k,l) + Rq_s(k,l)] \tag{3.20}$$

The value of $C$ can be approximated to

$$C = \frac{i+j}{AvgCh} \tag{3.21}$$

Thus, the service rate $\mu(i,j)$ of the system can be computed from Equation 3.19. Probability that a call leaves in time $dt$ is given by $\mu(i,j)dt$. When a call arrives, the system moves from state $(i,j)$ to state $(i + Rq_m(k,l), j + Rq_s(k,l))$ if the source and destination nodes are in positions $k$ and $l$ or vice versa. Thus,

$$Tr((i,j),(i + Rq_m(k,l), j + Rq_s(k,l))) = PR(k,l) \times \nu dt \tag{3.22}$$

for all possible regions $k$ and $l$ of source and destination nodes.

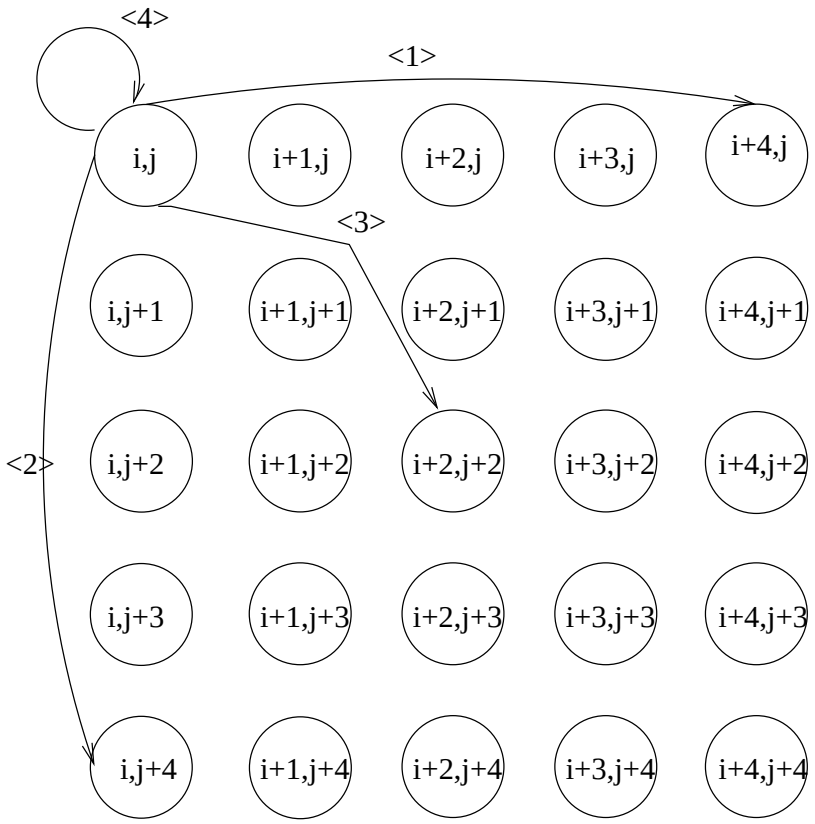


Figure 3.4: Some of the possible transitions of the Markov process from state (i,j)

For example, consider a portion of the Markov chain around state $(i, j)$ shown in Figure 3.4. The transition labeled 1 in the Figure represents the scenario when the source and destination nodes of the arriving call are within the subcell of radius $r$ around the BTS. In this case, the system needs 4 multihop channels to set up the source and destination uplink and downlink calls. Hence the system moves to state $(i + 4, j)$ after such a call is accepted. Thus the transition probability from state $(i, j)$ to state $(i + 4, j)$ is equal to the probability that a call arrives multiplied by the probability that the source and destination nodes are both in region 1. Thus the value of the transition probability for the arc labeled 1 in Figure 3.4 is given by $PR(1, 1) \times \nu dt$. Similarly, the arc labeled 2 represents the case when the source and destination nodes of the arriving calls are both in region 4 and hence require 4 single hop channels to establish a call. Thus the value of the transition probability for the arc labeled 2 in Figure 3.4 is given by $PR(4, 4) \times \nu dt$. The arc labeled 3 represents the case where one of the nodes of the arriving call connects to the BTS through a one hop path and the other node uses a single hop channel. Thus, 2 multihop channels and 2 single hop channels are required to establish such a call and thus the system moves from state $(i, j)$ to state $(i + 2, j + 2)$. Thus the value of the transition probability for the arc labeled 1 in Figure 3.4 is given by $PR(1, 4) \times \nu dt$.

Similarly, when a call leaves a system, the system moves from state $(i, j)$ to state $(i - Rq_m(k, l), j - Rq_s(k, l))$ if the source and destination nodes are in regions $k$ and $l$ or vice versa. Thus,

$$Tr((i, j), (i - Rq_m(k, l), j - Rq_s(k, l))) = PR(k, l) \times \mu(i, j)dt \tag{3.23}$$

for all possible regions $k$ and $l$.

If neither a call arrival nor a call departure takes place in the time $dt$, then the system remains in state $(i, j)$. Thus,

$$Tr((i, j), (i, j)) = 1 - \mu(i, j)dt - \nu dt \tag{3.24}$$

For example, in Figure 3.4, this transition is represented by the arc labeled 4.

After filling up the transition probability matrix for all possible transitions due to call arrival and call departure, all other transition probabilities from state $(i, j)$ are set to zero. In this way, the transition probability matrix is filled for all the $(M+1)(S+1)$ possible states. Note that, here we have assumed that, $(i + Rq_m(k, l), j + Rq_s(k, l))$ and $(i - Rq_m(k, l), j - Rq_s(k, l))$ are all valid states. Hence the above equations do not hold for the boundary cases. Appropriate changes are to be made to the above equations when filling the transition probability matrix at the boundaries. That is, if the transition cannot take place due to unavailability of channels, (say, if $i + Rq_m(k, l) > M$) then the corresponding transition probability matrix entry is set to zero. Also note that, if there is more than one way of transition between two states (for example, we can go from $(i, j)$ to $(i + 8, j)$ either if the source and destination are in regions 1 and 3 or if both the source and destination are in region 2), the corresponding transition probabilities should be added up and filled in the matrix.

After filling up the transition probability matrix, the steady state probabilities $Busy(i, j)$ can be solved for from the Equations 3.17 and 3.18 and the value of the CAR can be obtained from Equation 3.13.

## 3.2 Analysis of TWiLL System with Traffic Locality

Now, consider the scenario when the locality of the calls is not 1. The call is local (*i.e.*, the destination node is within the cell) with a probability $L$. In the case of local calls, the analysis remains as above. But in the case of non local calls, only the source uplink and source downlink calls need to be established. Thus for every region $k$ of the source, only $Rq_m(k)$ and $Rq_s(k)$ number of channels will be required to setup a call.

We now rewrite the Equation 3.13 for call acceptance ratio by accommodating the non local calls also. The Call Acceptance Ratio is now given as

$$\begin{aligned} CAR = L \sum_k \sum_l PR(k, l) Free(Rq_m(k, l), Rq_s(k, l)) + \\ (1 - L) \sum_k PR(k) Free(Rq_m(k), Rq_s(k)) \end{aligned} \tag{3.25}$$

The variable $AvgCh$ in Equation 3.20 is also modified as

$$\begin{aligned} AvgCh = L \sum_k \sum_l PR(k,l)[Rq_m(k,l) + Rq_s(k,l)] \\ +(1-L) \sum_k PR(k)[Rq_m(k) + Rq_s(k)] \end{aligned} \tag{3.26}$$

The transition probability matrix entries are also modified to accommodate non local calls. When a new call arrives, the next state of the system depends on whether the new call is local or non local. Thus, when the system is in state $(i,j)$, if a local call arrives, Equation 3.22 is rewritten as

$$Tr((i,j),(i + Rq_m(k,l), j + Rq_s(k,l))) = L \times PR(k,l)\nu dt \tag{3.27}$$

for all possible regions $k$ and $l$.

If a non local call arrives, only the 2 (source uplink and source downlink) out of the 4 calls need to be setup. Thus,

$$Tr((i,j),(i + Rq_m(k), j + Rq_s(k))) = (1-L) \times PR(k)\nu dt \tag{3.28}$$

for all possible regions $k$.

In the case when a local call departs,

$$Tr((i,j),(i - Rq_m(k,l), j - Rq_s(k,l))) = L \times PR(k,l)\mu(i,j)dt \tag{3.29}$$

for all possible regions $k$ and $l$.

Similarly, in the case when a non local call departs,

$$Tr((i,j),(i - Rq_m(k), j - Rq_s(k))) = (1-L) \times PR(k)\mu(i,j)dt \tag{3.30}$$

for all possible regions $k$.

If neither a call arrival nor a call departure takes place in the time $dt$, then the system remains in state $(i,j)$. Equation 3.24 remains unchanged for this case. The rest of the analysis remains the same as in the case where locality was 1. In this way, the call acceptance ratio can be obtained in the case when locality is not equal to one.

### 3.3 Analysis of a TWiLL System with Shortcut Relaying

Now let us consider a TWiLL system that supports shortcut relaying for local calls. When a local call arrives in a system, it is checked if a direct multihop path exists from the source to the destination, and if it does, the source and destination directly connect to each other without support from the BTS. This method consumes lesser channels and thus improves call accepting probability.
Let $PrSh(k)$ denote the probability that a shortcut path of length $k$ exists between the source and destination of a local call. We first compute the values of $PrSh(k)$ for $k = 1, 2$ and 3.

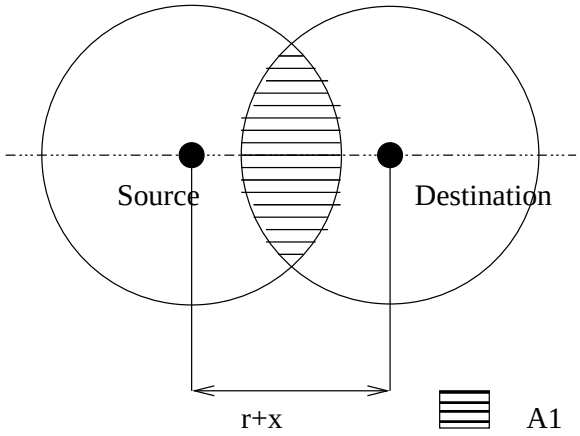


Figure 3.5: Calculating the probability that a two hop shortcut path exists

A shortcut path of length 1 exists from the source to the BTS if the destination is within a distance of $r$ from the source, *i.e.*, if the destination exists within an area of $\pi r^2$ around the cell. Thus the probability that a shortcut path of length 1 exists is given by $PrSh(1) = (\frac{r}{R})^2$.

Now let us compute the probability that a two hop path exists between a source and a destination. Refer to Figure 3.5 shown above. Let the destination node be at a distance $r + x$ from the source node. The probability that the destination exists at a distance $r + x$ is given by $\frac{2\pi(r+x)dx}{\pi R^2}$. Let the area of overlap between the transmission ranges of the source and destination be $A_1(x)$. $A_1(x)$ is given by the Equation 3.3. Now, for a two hop path to exist, we require that alteast one node be present in the area $A_1(x)$ to relay. The probability that atleast one node exists in the area $A_1(x)$ is given by $1 - (1 - \frac{A_1(x)}{\pi R^2})^{N-1}$. Thus, the probability that a two hop path exists from a source to the destination is given by,

$$PrSh(2) = \int_0^r \frac{2\pi(r+x)dx}{\pi R^2}(1 - (1 - \frac{A_1(x)}{\pi R^2})^{N-1}) \tag{3.31}$$

We now find the probability that a 3 hop shortcut path is taken between the source and destination. For a three hop path to exist, atleast one node should be present within a circle of radius $r$ around the cell and this node should have a two hop path to the destination. Probability that atleast one node is present within a circle of radius $r$ around a node is given by $1 - (1 - \frac{\pi r^2}{\pi R^2})^{N-1}$. A three hop shortcut path to the destination is taken when a two hop path does not exist, atleast one node exists within a distance $r$ of the source and a two hop path exists for this node. Thus,

$$PrSh(3) = (1 - PrSh(2))\times \quad (1 - (1 - \tfrac{\pi r^2}{\pi R^2})^{N-1}) \times PrSh(2) \tag{3.32}$$

We assume that only shortcut paths of lengths one, two and three are taken to the destination. Let $PrSh = PrSh(1) + PrSh(2) + PrSh(3)$ denote the probability that shortcut relaying is employed with any hoplength to reach the destination.

A shortcut path of length $k$ consumes $2k$ multihop channels (for the uplink and downlink calls) and zero single hop channels. Thus, the Equation 3.13 for call acceptance ratio can now be modified as

$$CAR = L\sum_{k}[PrSh(k)Free_m(2k)] + L(1-PrSh)\sum_{k}\sum_{l}[PR(k,l)$$
$$Free(Rq_m(k,l), Rq_s(k,l))] + (1-L)\sum_{k}[PR(k)Free(Rq_m(k), Rq_s(k))] \quad (3.33)$$

The first term in the above sum $L\sum_k[PrSh(k)Free_m(2k)]$ represents the probability that the call is local, a shortcut path exists between source and destination and multihop channels are free along the path. The second term $L(1-PrSh)\sum_k\sum_l$ $[PR(k,l)Free(Rq_m(k,l), Rq_s(k,l))]$ represents the probability that the call is local, a shortcut path does not exist and source and destination uplink and downlink calls are successfully setup through the BTS. The third term in the above equation $(1-L)\sum_k[PR(k)Free(Rq_m(k), Rq_s(k))]$ represents the probability that the call is non local and the source uplink and downlink calls are setup. This formula comprehensively covers all the possible cases when a call can be successfully setup in a TWiLL system.

The variable $AvgCh$ in Equation 3.20 is modified as follows to accommodate shortcut calls. Note that, a shortcut call of hop length $k$ consumes $2k$ multihop channels.

$$AvgCh = L\sum_{k}[2kPrSh(k)] + L(1-PrSh)\sum_{k}\sum_{l}[PR(k,l)(Rq_m(k,l) +$$
$$Rq_s(k,l))] + (1-L)\sum_{k}[PR(k)(Rq_m(k) + Rq_s(k))] \quad (3.34)$$

The transition probability matrix entries are also modified to accommodate shortcut calls. In the case when a new call arrives, the next state of the system depends on whether the new call is local and shortcut, local and non shortcut or non local. Thus, when the system is in state $(i,j)$, if a local shortcut call arrives,

$$Tr((i,j),(i+2k,j)) = L \times PrSh(k) \times \nu dt \quad (3.35)$$

for all possible values of $k$.

Equation 3.27 is rewritten as

$$Tr((i,j),(i+Rq_m(k,l), j+Rq_s(k,l))) =$$
$$L \times (1-PrSh) \times PR(k,l) \times \nu dt \quad (3.36)$$

for all possible regions $k$ and $l$.

Equation 3.28 remains as earlier.

For the case when a shortcut local call departs,

$$Tr((i,j),(i-2k,j)) = L \times PrSh(k) \times \mu(i,j)dt \quad (3.37)$$

for all possible values of $k$.

Equation 3.29 is rewritten as

$$Tr((i,j),(i - Rq_m(k,l), j - Rq_s(k,l))) = \\ L \times (1 - PrSh) \times PR(k,l) \times \mu(i,j)dt \tag{3.38}$$

for all possible regions $k$ and $l$.

Equations 3.30 and 3.24 remain unchanged. Other parts of the analysis are similar to the earlier sections. After filling up the transition probability matrix, we can proceed to solve for the steady state probabilities $Busy(i,j)$ from Equations 3.17 and 3.18 and thus solve for the call acceptance ratio from Equation 3.33.

### 3.4 Free Space Propagation Model

So far, we have assumed that the propagation at the radio layer is a free space propagation. The free space propagation model is used to predict received signal strength when the transmitter and receiver have a clear, unobstructed line-of-sight path between them. This is the model we have used in our simulations and analyzes until this point. The free space power received by a receiver antenna which is separated from the transmitter by a distance $d$ is given by the Friis space equation

$$P_r(d) = \frac{P_t G_t G_r \lambda^2}{(4\pi)^2 d^2} \tag{3.39}$$

where $P_t$ is the transmitted power, $P_r(d)$ is the received power which is a function of the T-R separation, $G_t$ is the transmitter antenna gain, $G_r$ is the receiver antenna gain, $d$ is the T-R separation distance in meters, and $\lambda$ is the wavelength in meters.

The *path loss*, which represents signal attenuation as a positive quantity measured in dB, is defined as the difference (in dB) between the effective transmitted power and the received power. The path loss for the free space model is given by,

$$PL(dB) = 10 \log \frac{P_t}{P_r} = -10log[\frac{G_t G_r \lambda^2}{(4\pi)^2 d^2}] \tag{3.40}$$

Furthermore, it is clear that Equation 3.39 does not hold for $d = 0$. For this reason, large scale propagation models use a close-in distance $d_0$, as a known received power reference point. The received power, $P_r(d)$, at any distance $d > d_0$, may be related to $P_r$ at $d_0$. The value $P_r(d_0)$ may be predicted from Equation 3.39, or may be measured by experiment. The received power at a distance $d$ greater than $d_0$ is given by,

$$P_r(d) = P_r(d_0)(\frac{d_0}{d})^2 \tag{3.41}$$

The path loss at a distance $d$ is thus given by

$$PL(d) = PL(d_0) + 20\log(\frac{d_0}{d}) \tag{3.42}$$

The free space propagation models is inadequate in predicting the path loss in real life situations which involve phenomena like reflection, diffraction, scattering and multipath propagation. Hence, we now modify our analysis to reflect these phenomena. In the subsequent sections, we introduce different propagation models, both empirical and analytical, and observe their effect on CAR.

We now describe how these propagation models fit into the analysis and simulation of the TWiLL system that we have been describing till this point. It has been described earlier in Chapter 2 that the nodes and the BTS continuously transmit beacons to build the incidence and interference matrices. Due to the introduction of propagation models in the simulations, the received power of the beacons is affected and thus the incidence matrix is affected. This in turn affects the formation of multihop paths between nodes and thus Call Acceptance Ratio (CAR) changes. We observe the effect of these propagation models on the CAR and on other parameters like multihop connectivity and average hop length. In the analysis, the propagation models determine the radio coverage area of a node and thus determine the scaling factor for multihop channels and some variables like $PR(i)$ described in Section 3.1.

We now begin with the first empirical model.

### 3.5 Log Distance Path Loss Model

Measurements indicate that average received signal power decreases logarithmically with distance. The average path loss can be expressed as a function of distance using a path loss exponent $n$.

$$PL(dB) = PL(d_0) + 10n\log(\frac{d}{d_0}) \tag{3.43}$$

where $n$ is the path loss exponent which indicates the rate at which the path loss increases with the T-R separation distance. The path loss values in the above equation denote the ensemble average of all possible path loss values for a given value of $d$. The value of $n$ depends on the specific propagation environment. For example, in free space, $n$ is equal to 2, and when obstructions are present, $n$ will have a larger value. We now analyze a TWiLL system where the radio channel propagation follows the log distance model.

The path loss exponent affects the path loss over every transmission and thus reduces the effective transmission radius of multihop and single hop transmissions. However we assume that the transmission power is increased in a such a way that the single hop coverage area is not effected by the path loss exponent. This assumption is justified because the transmissions over the control channel i.e., single hop channels

are crucial in maintaining state information like incidence and interference matrices. Reduction in the coverage area of single hop transmissions might result in some nodes not receiving the beacon from the BTS and thus getting isolated. Thus, we observe the effect of the path loss exponent only due to change in multihop transmission coverage area.

Let the *effective multihop radius* after the introduction of the path loss exponent be $r_{eff}(n)$. The effective radius is defined as the distance from the transmitter at which the signal strength reduces to the level of the signal strength at the boundary $r$ in the free space model. Let $P_{CST}$ be the carrier sensing threshold. The transmission power of the nodes is set to such a value that the received power at the nodes, assuming free space propagation, is just equal to $P_{CST}$. The multihop transmission power $P_t$ is thus given by,

$$P_t = P_{CST} + PL(d_0) + 20\log(\frac{r}{d_0}) \tag{3.44}$$

In the new propagation model, the received power at $r_{eff}(n)$ is equal to $P_{CST}$.

$$P_r(r_{eff}(n)) = P_t - PL(d_0) - 10n\log(\frac{r_{eff}(n)}{d_0}) = P_{CST} \tag{3.45}$$

Substituting for $P_t$ from Equation 3.44 in 3.45 we obtain,

$$2\log(\frac{r}{d_0}) = n\log(\frac{r_{eff}(n)}{d_0}) \tag{3.46}$$

Solving for $r_{eff}(n)$,

$$r_{eff}(n) = (\frac{r}{d_0})^{\frac{2}{n}} \times d_0 \tag{3.47}$$

By substituting the value of $r_{eff}(n)$ for $r$ in Equations 3.2, 3.4, 3.9, 3.10, we can obtain a theoretical estimate of CAR when the log distance propagation model is used, the only difference being that we need to consider paths of hop length greater than 3 also as the value of $n$ increases. The rest of the analysis remains exactly the same.

We also calculate two other parameters analytically - the average hop length of any path and the cardinality of Set B. Set B is defined as the set of nodes that are isolated in the multihop connectivity graph. The average hop length can be calculated using a weighted average of all possible hop lengths by using as weights the probabilities that paths of that hop length exist. These probabilities can be obtained from the values $PR(i)$ computed in this chapter. To obtain the cardinality of the Set B, we calculate

the probability that the node belongs to Set B (i.e., the probability that the node has no multihop neighbors) and multiply this probability by the number of nodes in the system. A node has no multihop neighbors if all other $N-1$ nodes of the system lie outside the transmission range of the cell. Let $A$ denote the transmission area of a node. It is equal to the area of a circle of radius $r$. Then the probability $P_{SetB}$ that a node belongs to Set B is given by

$$P_{SetB} = (1 - \frac{A}{\pi R^2})^{N-1} \tag{3.48}$$

Thus the cardinality of Set B $N_{SetB}$ can be calculated as

$$N_{SetB} = P_{SetB} \times N \tag{3.49}$$

## 3.6 Log Normal Shadowing Model

The log distance model does not consider the fact that the surrounding environment may be vastly different in two different locations with the same T-R separation. This leads to measured signals which are vastly different from the average value predicted by the log distance model. Measurements have shown that at any value of $d$, the path loss $PL(d)$ at a particular location is random and distributed log-normally (normal in dB) about the mean distance dependent value. That is,

$$PL(d) = PL(d) + X_\sigma = PL(d_0) + 10n\log(\frac{d}{d_0}) + X_\sigma \tag{3.50}$$

and

$$P_r(d) = P_t - PL(d) \tag{3.51}$$

where $X_\sigma$ is a zero mean Gaussian distributed random variable (in dB) with standard deviation $\sigma$ (also in dB).

The log normal distribution describes the random shadowing effects which occur over a large number of measurement locations which have the same T-R separation but have different levels of clutter in the propagation path. This phenomenon is referred to as *log normal shadowing*. In practice, the values of $n$ and $\sigma$ are computed from measured data using linear regression.

Since $PL(d)$ is a random variable with a normal distribution in dB about the distance dependent mean. The Q-function or error function (erf) may be used to determine the probability that the received signal will exceed a particular threshold. The Q-function is defined as

$$Q(z) = \frac{1}{\sqrt{2\pi}} \int_z^\infty \exp(-\frac{x^2}{2})dx = \frac{1}{2}(1 - erf(\frac{z}{\sqrt{2}})) \tag{3.52}$$

where $Q(z) = 1 - Q(-z)$.

The probability that the received signal level will exceed a certain threshold $\gamma$ can be calculated from the cumulative density function as

$$Pr(P_r(d) > \gamma) = Q(\frac{\gamma - P_r(d)}{\sigma}) \tag{3.53}$$

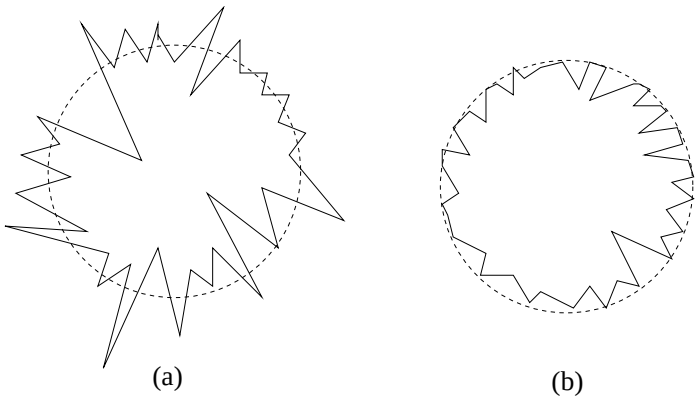


Figure 3.6: Effect of sigma on the cell boundary (a) Unrestricted case (b) Restricted case

Due to the addition of the random noise component, the coverage area of a node gets distorted, as shown in the Figure 3.6(a). Since the random noise variable $X_\sigma$ can take negative values also, nodes beyond the transmission radius also become reachable in some cases. However, if we assume that nodes beyond the original transmission radius cannot be reached, then the coverage area becomes as shown in Figure 3.6(b). We will call the first case the unrestricted case and the second case as the restricted case. We will observe the effect of $\sigma$ on performance in these two cases.

As in Section 3.5, change in the coverage area of control channels can lead to adverse effects. When a random noise component is also introduced on the control channel, many problems arise. For example, due to random effects, a node might get a beacon from another BTS, in addition to its nearest BTS. This leads to incorrect state information in the system. Thus we assume that the shadowing effects are absent in all transmissions over the control channel. This can be realized by suitably increasing the transmission power. This ensures correct topology information. Thus the effects of shadowing are observed only on data transmissions over multihop channels.

### 3.6.1 The unrestricted case

In the unrestricted case, the coverage area of a multihop transmission is as shown in Figure 3.6(a). As in Section 3.5, we calculate the effective radius of transmission. Let $r_{eff}(\sigma)$ be the effective radius of transmission. We will obtain its value in terms of

the $r$, the multihop transmission radius when free space propagation model is used. Equating the power at the boundary in both cases, as in Equation 3.45,

$$P_t - PL(d_0) - 10n\log(\frac{r_{eff}(\sigma)}{d_0}) - X_\sigma = P_t - PL(d_0) - 20\log(\frac{r}{d_0}) \tag{3.54}$$

Simplifying, we have,

$$r_{eff}(\sigma) = (\frac{r}{d_0})^{\frac{2}{n}} \times d_0 \times 10^{-\frac{X_\sigma}{10n}} \tag{3.55}$$

Taking the expected value of the random variable and substituting for $r_{eff}(n)$ from Equation 3.47, we obtain

$$r_{eff}(\sigma) = r_{eff}(n) \times E(10^{-\frac{X_\sigma}{10n}}) \tag{3.56}$$

where $E(.)$ denotes the expected value of a random variable. The problem now boils down to finding the expected value of the function $f(x) = 10^{-\frac{x}{10n}}$ where $x$ is a random variable with mean $\mu = 0$ and standard deviation $\sigma$. The rest of the section is devoted to this issue.

We now that any continuous function $f(x)$ may be expressed as

$$f(x) = f(\mu) + (x-\mu)f'(\mu) + \frac{1}{1.2}(x-\mu)^2 f''(\mu) + \frac{1}{1.2.3}(x-\mu)^3 f'''(\mu) + \ldots \tag{3.57}$$

In the case when $x$ is a random variable with mean $\mu$ and standard deviation $\sigma$, according to [24],

$$E(f(x)) = f(x) + \frac{1}{2}\sigma^2 f''(x) + \ldots \tag{3.58}$$

By expanding in differences rather than in derivatives, we obtain,

$$\begin{aligned} f(x) = f(\mu) + (x-\mu)(\frac{f(\mu+h) - f(\mu-h)}{2h}) + \\ \frac{1}{2}(x-\mu)^2(\frac{f(\mu+h) - f(\mu) + f(\mu-h)}{h^2}) + \ldots \end{aligned} \tag{3.59}$$

which gives the approximation

$$E(f(x)) = f(\mu) + \frac{\sigma^2}{2}(\frac{f(\mu+h) - 2f(\mu) + f(\mu-h)}{h^2}) \tag{3.60}$$

In [25], it was suggested that an appropriate choice for $h$ is $\sqrt{3}\sigma$ which yields

$$E(f(x)) = \frac{2}{3}f(\mu) + \frac{1}{6}f(\mu + \sqrt{3}\sigma) + \frac{1}{6}f(\mu - \sqrt{3}\sigma) \tag{3.61}$$

Using this approximation to evaluate the effective radius, we have

$$r_{eff}(\sigma) = r_{eff}(n) \times (\frac{2}{3} + \frac{1}{6}10^{\frac{-\sqrt{3}\sigma^2}{10n}} + \frac{1}{6}10^{\frac{\sqrt{3}\sigma^2}{10n}}) \tag{3.62}$$

Once the effective radius is computed as described above, the analysis is similar to that done earlier in Section 3.5.

### 3.6.2 The restricted case

In the restricted case, the coverage area of a multihop transmission is as shown in Figure 3.6(b). As in Section 3.5, we calculate the effective radius of transmission. Let $r_{eff}(\sigma)$ be the effective radius of transmission. Due to random effects of shadowing, some locations within a coverage area of a multihop transmission will be below the carrier sensing threshold $\gamma$. Let $U(\gamma)$ denote the fraction of the circle or radius $r$ that is affected by the transmission. Since the area of a circle is proportional to the square of its radius, the effective radius $r_{eff}(\sigma)$ can be calculated as

$$r_{eff}(\sigma) = r \times \sqrt{U(\gamma)} \tag{3.63}$$

Once the effective radius is computed, the rest of the analysis is similar to Sections 3.5 and 3.6. All that remains to be computed is the variable $U(\gamma)$.

From [16], we obtain $U(\gamma)$ as

$$U(\gamma) = \frac{1}{2}(1 - erf(a) + exp(\frac{1-2ab}{b^2})(1 - erf(\frac{1-ab}{b}))) \tag{3.64}$$

where

$$a = \frac{\gamma - P_t + PL(d_0) + 10n\log(\frac{r}{d_0})}{\sigma\sqrt{2}} \tag{3.65}$$

and

$$b = \frac{10n\log e}{\sigma\sqrt{2}} \tag{3.66}$$

In our case, the threshold is set as the signal level at a distance $r$ i.e., $\gamma = P_t + PL(d_0) + 10n\log(\frac{r}{d_0})$. Thus $a = 0$. So, we have

$$U(\gamma) = \frac{1}{2}(1 + exp(\frac{1}{b^2})(1 - erf(\frac{1}{b}))) \tag{3.67}$$

Thus, the effective radius is obtained as,

$$r_{eff}(\sigma) = r \times \sqrt{(\frac{1}{2}(1 + exp(\frac{1}{b^2})(1 - erf(\frac{1}{b}))))} \tag{3.68}$$

After obtaining the effective radius, we proceed with the analysis as in the earlier sections.

### 3.7 Walfisch and Bertoni Model

We now examine an analytical propagation model. The Walfisch Bertoni (WB) model provides the value of path loss as a result of propagation of buildings and streets. Building and street parameters involved in the path loss calculation are average height of intervening buildings and average spacing of neighbouring building rows. It is assumed that buildings are the only terrain features present. Note that the WB model is an analytical model and hence computes path loss by considering the phenomena of diffraction and scattering of the propagating wave by the intervening buildings.

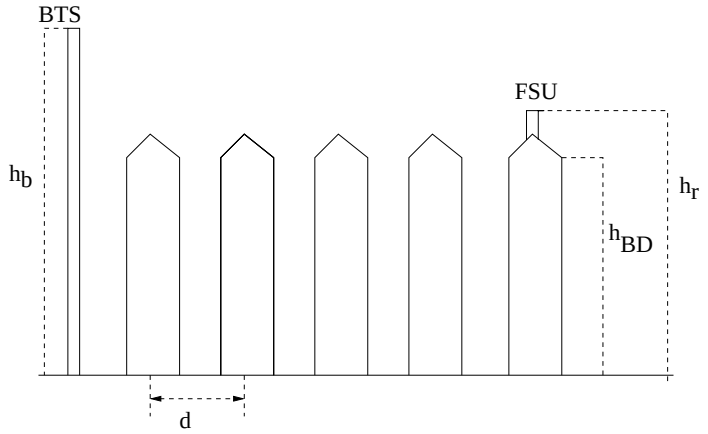


Figure 3.7: Walfisch Bertoni Model

Let the average building height be $h_{BD}$, as shown in Figure 3.7. Let $h_b$ be the height of the transmitting antenna i.e., the antenna of the BTS. Let $h_r$ be the antenna height at the receiver. Relative antenna heights $\delta h_b$ and $\delta h_r$ are given by

$$\delta h_b = h_b - h_{BD} \tag{3.69}$$

and

$$\delta h_r = h_{BD} - h_r \tag{3.70}$$

Overall path loss $PL$ in dB can be approximated by the summation of

- Free space path loss $L_0$
- Loss due to multiple screen diffraction at intervening buildings $L_{msd}$
- Loss due to scattering at the last rooftop $L_{rts}$

In this report, we consider only a simplified version of the WB model, where the receiver antenna is directly mounted over the receiver rooftop and the relative height of the antenna over the rooftop is negligible. In such a scenario, the last term $L_{rts}$ becomes insignificant.

The free space path loss $L_0$ is computed as $PL(r)$ in Section 3.4.

$$L_0 = PL(d_0) + 20n \log \frac{r}{d_0} \tag{3.71}$$

The path loss due to diffraction at the intervening buildings is given by

$$L_{msd}(r) = -10 \log Q^2(g_p) \tag{3.72}$$

where

$$Q(g_p) = 2.35 g_p^{0.9} \tag{3.73}$$

and

$$g_p = \frac{\delta h_b}{r} \sqrt{\frac{d}{\lambda}} \tag{3.74}$$

where $d$ is the average spacing between buildings and $r$ is the radius of transmission.

We now proceed to find the effective radius of transmission, as was the case with other models. The effective radius $r_{wb}$ is given by

$$L_{msd}(r_{wb}) + PL(r_{wb}) = PL(r) \tag{3.75}$$

Simplifying, we get

$$-\log(2.35(\frac{\delta h_b}{r_{wb}} \sqrt{\frac{d}{\lambda}})^{0.9}) + \log \frac{r_{wb}}{d_0} = \log \frac{r}{d_0} \tag{3.76}$$

from which we can solve for the effective radius $r_{wb}$. After solving for the effective radius, the rest of the analysis remains the same as in the earlier sections.

### 3.8 Simulation Results

To verify the call acceptance ratio values that were obtained through analysis, we simulated a TWiLL system using GloMoSim [26]. The system consisted of 11 cells, grouped into clusters of 3, spread over a terrain of dimensions 2.01 km $\times$ 2.61 km. Every cluster of three cells had 42 data channels - both multihop and single hop. The radius of single hop transmission (*i.e.*, the radius of the cell) was 500 m and the radius of multihop transmission was 250 m. The simulation was run for 3 minutes and with 300 nodes in the system. The arrival rate of calls was controlled by changing the mean inter call arrival time $I$. The default value was 30 seconds *i.e.*, every node made a call every 30 seconds. The default mean call holding time $h$ was 19 seconds. The Erlang traffic in each cell with $N_{cell}$ number of nodes is given by

$$T_{cell} = \frac{N_{cell} \times h}{I} \tag{3.77}$$

The value of locality was taken to be equal to one in all simulations except in the simulations in which locality was varied. Every simulation was run over many seeds. The ratio of the number of calls accepted to the number of calls made was averaged over all the seeds. The results are as shown below.

In the comparison of the analysis and simulation values shown below, it is observed that the values obtained from simulation are always lower than the values obtained from analysis. One possible reason for this deviation could be that, in the analysis, we have assumed that a multihop channel can be reused as per Equation 3.12 within a cell. But this is not always feasible. Thus the effective number of multihop channels is in reality less than the calculated value and thus the analysis values act as a theoretical upper bound for the simulation values. And hence, the simulation values will always be lower than the analysis values.

We have also computed the call acceptance ratio values for a traditional WiLL system under similar conditions, both from simulation and from analysis (using Equation 3.14). These values have been included along with the values of a TWiLL system to illustrate the throughput enhancement achieved by the TWiLL architecture.

#### 3.8.1 Call Acceptance Ratio vs Mean Call Holding Time

The load on the TWiLL system was varied by varying the mean call holding time (or the mean service time of the calls) from a minimum of 1 second to a maximum of 23 seconds. 39 of the data channels operated in the multihop mode and 3 in the single hop mode. Locality of traffic was kept at 1. A comparison of the analysis and simulation values is as shown in Figure 3.8. It is observed that the call acceptance ratio decreases sharply with increase in load when shortcut relaying was not used, which is the expected trend. In the case when shortcut relaying was used, the call acceptance ratio was higher and fell less sharply at higher loads. We note that the analysis values are slightly higher than the simulation values in both cases, as explained in

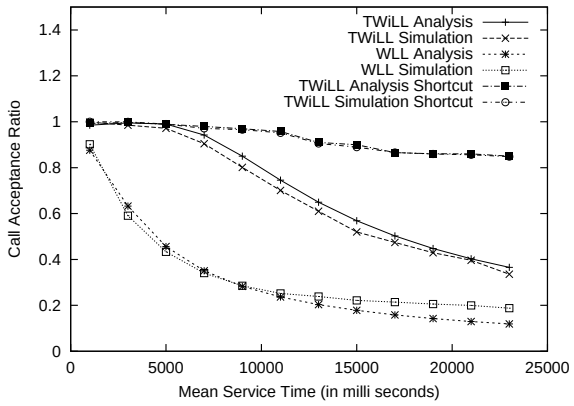


Figure 3.8: Call Acceptance Ratio vs Mean Call Holding Time

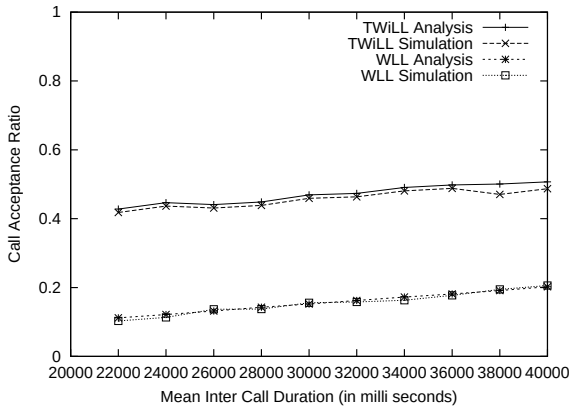


Figure 3.9: Call Acceptance Ratio vs Mean Inter Call Arrival Time

the earlier section. We also note that a TWiLL system gives a higher throughput than a traditional WiLL system under similar conditions.

### 3.8.2 Call Acceptance Ratio vs Mean Inter Call Arrival Time

The load on the TWiLL system was varied by varying the inter call arrival time of a node. The duration between calls was varied from 22 seconds to 40 seconds. The mean call holding time was fixed at 19 seconds. A comparison of the analysis and simulation values is as shown in the Figure 3.9. The call acceptance ratio increases as the mean duration between calls increases, which is the expected trend. The call acceptance values are lower for a WiLL system compared to a TWiLL system.

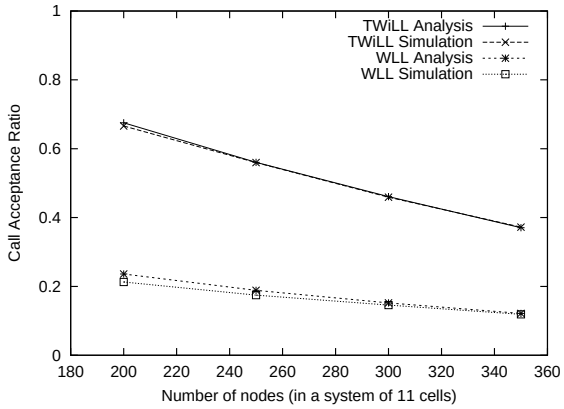


Figure 3.10: Call Acceptance Ratio vs Node Density

### 3.8.3 Call Acceptance Ratio vs Node Density

The simulations were run with 200, 250 and 300 nodes in the system. The mean call holding time was 19 seconds and the mean inter call arrival time for a node was 30 seconds. A comparison of the analysis and simulation values is as shown in the Figure 3.10. It can be observed that the call acceptance ratio decreases with increasing node density. The acceptance values are lower in a WiLL system compared to a TWiLL system as bandwidth reuse takes place in TWiLL.

### 3.8.4 Call Acceptance Ratio vs Number of Multihop Channels

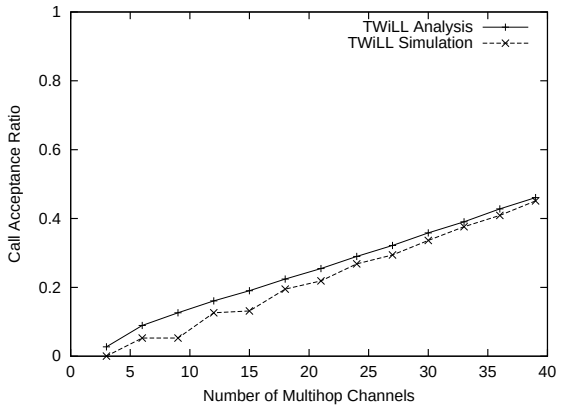


Figure 3.11: Call Acceptance Ratio vs Number of Multihop Channels

The number of multihop channels was varied from 0 to 42 and the effect on call acceptance ratio was observed. It can be observed from Figure 3.11 that the call

acceptance ratio goes to zero when there are zero multihop channels in the system, in spite of there being 42 single hop channels. This can be explained as follows. We have assumed that a single hop channel is used only when a multihop channel allocation fails. Thus, when a multihop path exists to the BTS but multihop channels are not available, a single hop channel is not tried. At the kind of node densities used in the simulation, a multihop path to the BTS almost always existed. Thus, single hop channels were rarely used to connect to the BTS and thus the call acceptance ratio approached zero as the number of multihop channels were reduced to zero.

### 3.8.5 Call Acceptance Ratio vs Locality

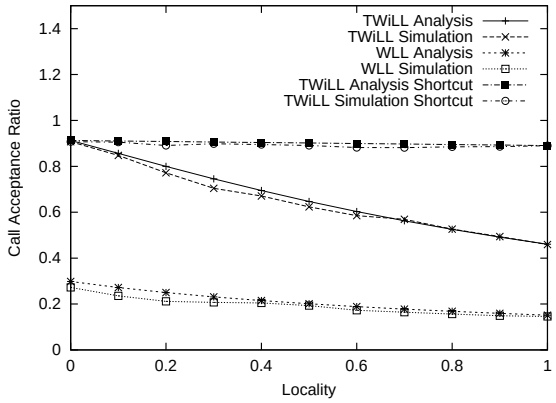


Figure 3.12: Call Acceptance Ratio vs Locality

The locality of the calls was varied from 0 to 1 on a TWiLL system that did not support shortcut relaying. When shortcut relaying is not supported, local calls consume more number of channels than non local calls (since, for a non local call, only the source uplink and source downlink calls need to be setup whereas, for a local call, even the destination uplink and destination downlink calls should be setup). Thus, as locality increases, the number of local calls increase and thus the call acceptance ratio decreases (as shown in Figure 3.12). This trend will reverse when shortcut relaying is supported. When there is shortcut relaying, the additional load on the system caused due to increasing locality is nullified by the reduction in load caused due to shortcut relaying of local calls. Thus we can see from Figure 3.12 that the call acceptance ratio increases with increasing locality when shortcut relaying is employed. We also observe the improvement in performance of a TWiLL system when compared to a traditional WiLL system.

### 3.8.6 Call Acceptance Ratio vs Path Loss exponent

Appropriate changes corresponding to the log distance model were made in the radio layer of GloMoSim and the simulations were run. As explained earlier, the coverage

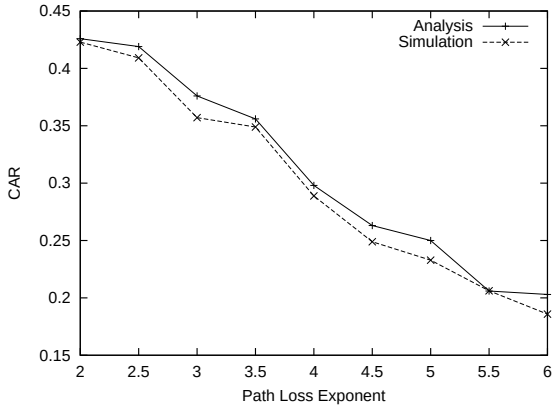


Figure 3.13: Call Acceptance Ratio vs Path Loss exponent

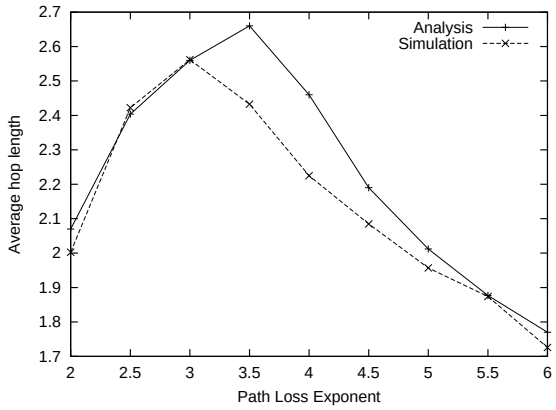


Figure 3.14: Average Hop Length vs Path Loss exponent

area of nodes over single hop channels was maintained at the original value of $R$ by increasing the transmission power in accordance with the path loss exponent. However, the transmission power over multihop channels was not changed with the path loss exponent. Thus the effect of the path loss exponent can be observed over multihop transmissions. The effect of the path loss exponent $n$ was observed over the following variables: CAR, average hop length and the cardinality of Set B. The value of $n$ was varied from 2 to 6 and the simulation and analysis results were compared.

It can be observed from Figure 3.13 that the CAR reduces with increasing $n$. As the value of $n$ increases, the effective multihop radius reduces. Thus, the average path length increases, as seen in Figure 3.14. This necessitates the use of more multihop channels. Though this is offset to a certain extent by increased reuse of multihop channels (since, now a multihop transmission effectively blocks lesser area), the CAR still reduces. This can also be explained by the increase in the cardinality of Set B,

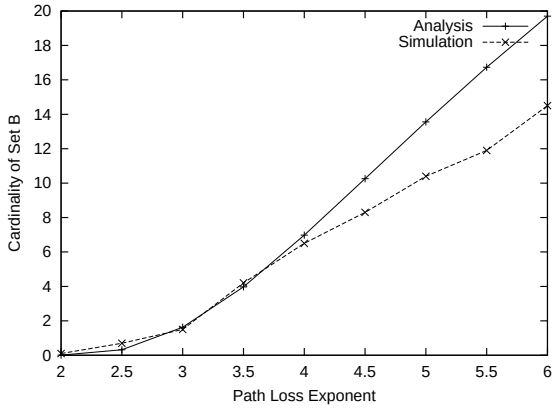


Figure 3.15: Cardinality of Set B vs Path Loss exponent

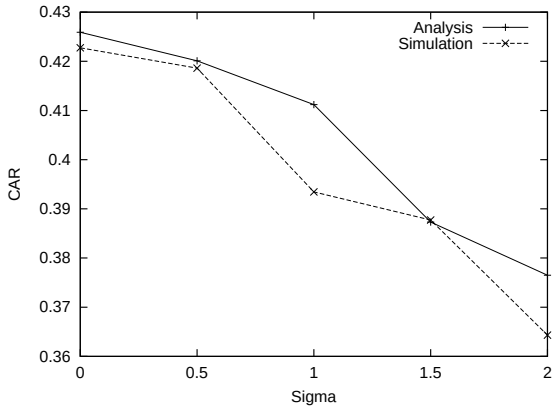


Figure 3.16: Call Acceptance Ratio vs Sigma - Unrestricted case

as seen in Figure 3.15 which reduces multihop connectivity and thus the formation of multihop paths.

### 3.8.7 Call Acceptance Ratio vs Sigma

The changes corresponding to the log normal model were incorporated into the radio layer of GloMoSim and the simulations were run.The value of $\sigma$ was varied between 0 and 2 and the effect on CAR and average hop length was observed.

In the unrestricted case, it can be observed from Figure 3.16 that the CAR decreases with increasing $\sigma$, which is justified since shadowing effects hinder multihop connectivity. Also, the effective radius increases with increasing $\sigma$, which can be deduced from the decreasing hop length, as shown in Figure 3.17.

In the restricted case, it can be observed from Figure 3.18 that the CAR decreases

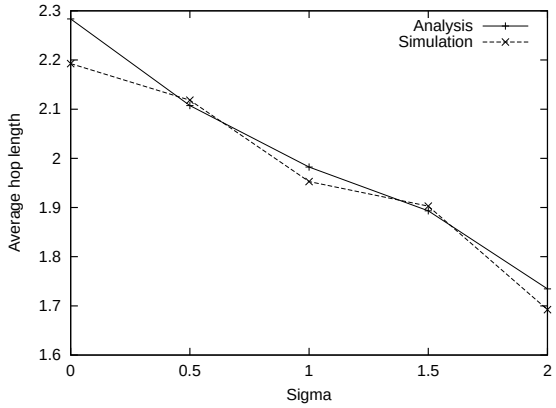


Figure 3.17: Average Hop Length vs Sigma - Unrestricted case

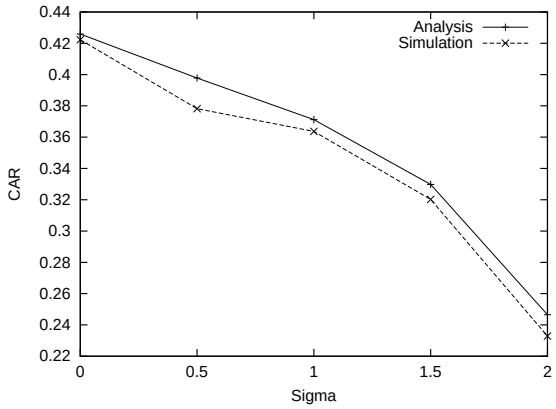


Figure 3.18: Call Acceptance Ratio vs Sigma - Restricted case

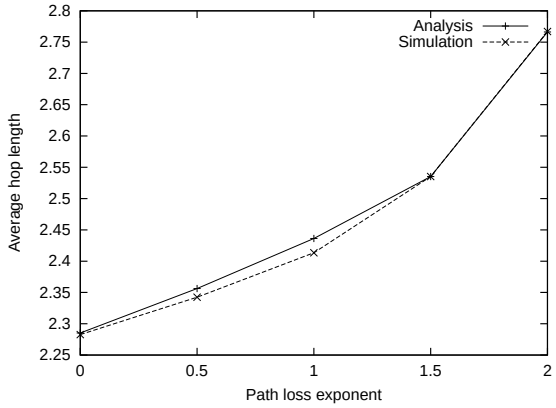


Figure 3.19: Average Hop Length vs Sigma - Restricted case

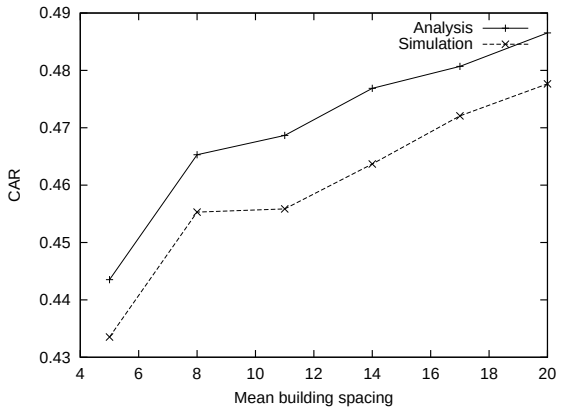


Figure 3.20: Call Acceptance Ratio vs Mean spacing between buildings

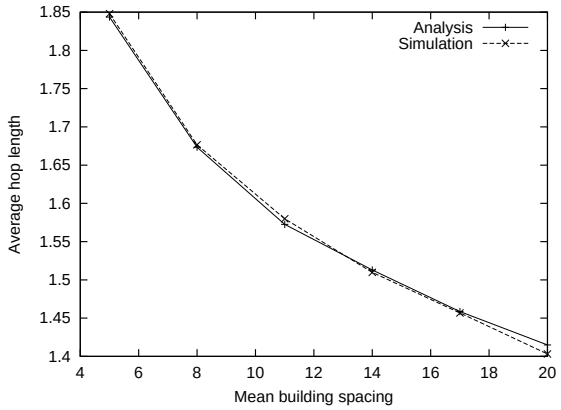


Figure 3.21: Average Hop Length vs Mean spacing between buildings

with increasing $\sigma$, which is justified since shadowing effects hinder multihop connectivity. But in this case, the effective radius decreases with increasing $\sigma$, which can be deduced from the increasing hop length, as shown in Figure 3.19. Note that the effect of $\sigma$ is more pronounced in the case of the restricted case than in the unrestricted case, which is justified since the area of coverage is more adversely affected in the restricted case.

### 3.8.8 Call Acceptance Ratio vs Terrain Parameters in WB model

The changes corresponding to the WB model were incorporated into the radio layer of GloMoSim and the simulations were run. The mean separation between buildings was varied by changing the parameter $\frac{d}{\lambda}$ between 5 and 20. The mean height of the buildings was also varied by changing the parameter $\delta h_b$ between 50 and 100.

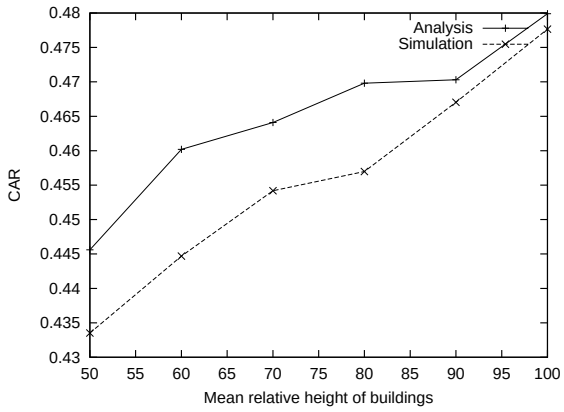


Figure 3.22: Call Acceptance Ratio vs Relative height of buildings

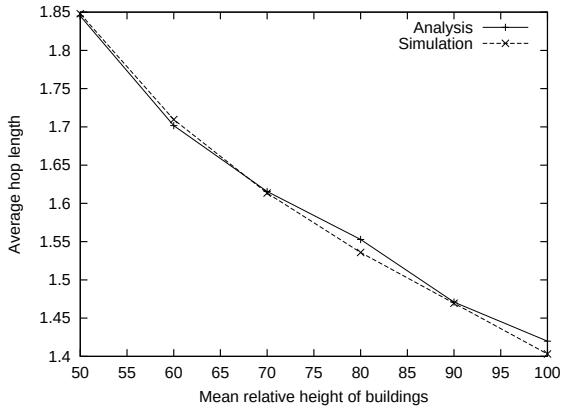


Figure 3.23: Average Hop Length vs Relative height of buildings

It can be observed from Figure 3.20 that the CAR increases with increasing $\frac{d}{\lambda}$, which is justified since closely packed buildings tend to cause more diffraction effects. Also, the effective radius increases with increasing $\frac{d}{\lambda}$, which can be deduced from the decreasing hop length, as shown in Figure 3.21.

It can be observed from Figure 3.22 that the CAR increases with increasing $\delta h_b$, which is justified since larger height difference between the BTS and the buildings causes lesser diffraction. Also, the effective radius increases with increasing $\delta h_b$, which can be deduced from the decreasing hop length, as shown in Figure 3.23.

# CHAPTER 4

# Performance Analysis of the DWiLL Architecture

In this chapter, we analytically derive the call accepting probability of a DWiLL system. The performance analysis of DWiLL follows along the lines of the analysis of TWiLL carried out in the previous chapter. Hence in this chapter, we will describe only the points where the analyzes differ. The portions of the analysis which differs from TWiLL are:

- Regions of the cell: The identification of various regions in a cell based on the hop length of the path between the nodes in the region and the BTS, as described in Section 3.1.1, will be different in a DWiLL system. The probabilities that one hop, two hop and three hop paths respectively exist from a node to the BTS will be different. Thus the values $PR(i)$ for possible values of $i$ will have to be recomputed.
- Number of channels required: The number of multihop and single hop channels required for the establishment of a subcall will be different in DWiLL from the values mentioned in Section 3.1.2. Thus the arrays $Rq_m$ and $Rq_s$ have to be recomputed.
- Scaling of multihop channels: The area blocked by a multihop transmission will be different from that computed in Section 3.1.3 since a DWiLL system employs directional multihop transmissions. Thus the effective number of multihop channels have to be recomputed.

Apart from the changes mentioned above, the remainder of the analysis is similar to the corresponding parts of the previous chapter. The analysis using propagation models, which involves the computation of the effective multihop radius, also remains the same.

## 4.1 Analysis of DWiLL

We now derive a mathematical expression for the call accepting probability of a simple DWiLL system with locality of 1 and without support for shortcut relaying. Analysis for systems with non local calls will be provided in the subsequent sections. In addition to the system parameters described in Section 3.1, we have a new parameter $\theta$, which is directionality of the transmissions.

### 4.1.1 Identification of various regions within a cell

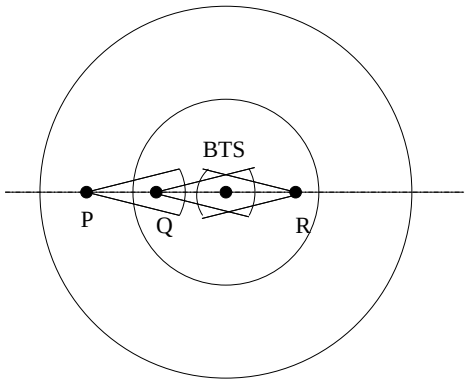


Figure 4.1: One hop and two hop paths from a node to the BTS

We now find the number of channels needed per call. The number of multihop and single hop channels needed depends upon the position of the source and destination nodes. A given node can exist in three possible regions. Region 1: The node is within the inner sub cell of radius $r$ and thus can reach the BTS using one multihop channel. Region 2: A two hop path exists from the node to the BTS. Region 3: No multihop path exists from the source to the BTS. So the node connects to the BTS via a single hop channel. We have assumed that a single hop channel is used only when a multihop path does not exist. A single hop channel is not tried when a multihop path exists but multihop channel allocation fails. This assumption is justified because single hop channels are meant to be used when a node gets isolated from the other nodes (this is called a partition) and thus cannot use any multihop channels. We have also assumed that the probability that a three hop multihop path exists between a node and the BTS is negligible. This assumption is justified since due to the directionality of the transmissions, multihop connectivity is low.

We now calculate the probabilities that a node is in the various possible regions of a cell. A node is in the above described region 1 if it is within the inner sub cell of radius $r$. Node R in Figure 4.1 is an example. Thus, $PR(1) = (\frac{r}{R})^2$

We now calculate the probability that a two hop path exists between a node and the BTS. This requires that the node is outside the sub cell of radius $r$ and an intermediate node is found within the region of overlap between the transmission range of the cell and the inner sub cell. P - Q - BTS is one such path in Figure 4.1. Probability that a node is at a distance $r + x$ from the center of the circle (for $x$ varying from 0 to $R - r$ ) is given by $\frac{2\pi(r+x)dx}{\pi R^2}$. Consider one such node that is at a distance of $r + x$ from the center of the cell. The inner sub cell of the cell and the sector of a circle of radius $r$ around the cell (in which the node can potentially transmit) intersect. Let the area of intersection be $A_1(x)$. The value of $A_1(x)$ depends on the value of $x$, as shown in Figure 4.2. Let $x_1$ be the value of $x$ that satisfies the

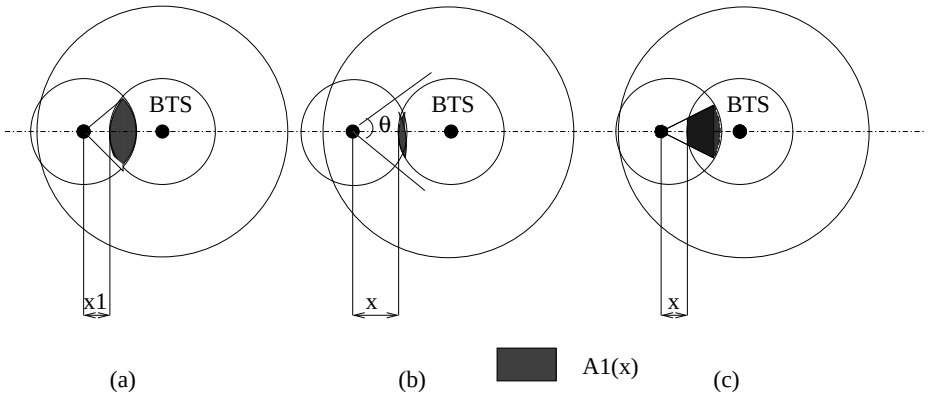


Figure 4.2: Two hop paths from a node to the BTS

equation

$$2 \times \arccos(\frac{r+x}{2r}) = \theta \tag{4.1}$$

This is shown in Figure 4.2(a). For values of $x \geq x_1$, $A_1(x)$ is equal to the area of overlap of two circles of radii $r$ separated by a distance $r + x$, as shown in Figure 4.2(b), and its value is given by the expression $r^2(q - \sin q)$ where $q = 2 \times \arccos(\frac{r+x}{2r})$. For values of $x < x_1$, $A_1(x)$ can be approximated to $\frac{1}{2}r^2\theta - \frac{1}{2}x^2\theta$, as shown in Figure 4.2(c). Now, for a multihop path to be found we require that at least one node exists in this area to connect to the BTS. For any node, the probability that it will not exist in this area is equal to $1 - \frac{A_1}{\pi R^2}$. Thus the probability that at least one out of the remaining $N - 1$ nodes exists in this area is given by $1 - (1 - \frac{A_1(x)}{\pi R^2})^{N-1}$. Thus, the average probability that a two hop path exists from a node to the BTS is given by the following integral.

$$PR(2) = \int_0^{R-r} \frac{2\pi(r+x)}{\pi R^2}(1 - (1 - \frac{A_1(x)}{\pi R^2})^{N-1})dx \tag{4.2}$$

A single hop channel is used only when a multihop path does not exist. Thus, the probability that a node uses a single hop channel to connect to the BTS is given by, $PR(3) = 1 - PR(1) - PR(2)$.

### 4.1.2 Number of channels required for the establishment of a call

We now estimate the number of channels needed for each location of the source and destination. As noted earlier, $Rq_m(k)$ and $Rq_s(k)$ are the number of multihop and single hop channels required to establish the source uplink and downlink calls when the source node is in position $k$, respectively. The values of $Rq_m(k)$ and $Rq_s(k)$ for all values of $k$ are given in Table 4.1 below. It is also indicated whether the multihop transmissions are used in omni directional mode or directional mode.

Table 4.1: Number of Channels Required to Establish a Call in a DWiLL System

| Region | $Rq_m$ | $Rq_s$ |
|---|---|---|
| 1 | 2 (1 Omni, 1 Directional) | 0 |
| 2 | 2 (Both Directional) | 1 |
| 3 | 0 | 2 |

As denoted earlier, let $Rq_m(k,l)$ and $Rq_s(k,l)$ be the number of multihop and single hop channels required for both uplink and downlink calls for the source and destination when the source and destination nodes are in positions $k$ and $l$ or $l$ and $k$. Obviously, $Rq_m(k,l)$ is equal to $Rq_m(k) + Rq_m(l)$. Similarly for $Rq_s(k,l)$.

### 4.1.3 Computing the effective number of multihop channels

Since a single transmission over a multihop channel does not block the entire cell, the effective number of multihop channels $M$ is different from the actual number of multihop channels $m$ in a cell. We now compute the effective number of multihop channels available.

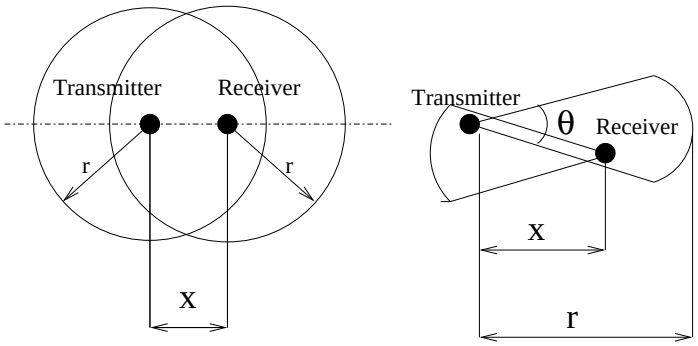


(a) Omni directional (b) Directional

Figure 4.3: Area blocked by a multihop transmission

When a multihop channel is used in the omni directional mode, the area blocked by the transmission is as shown in Figure 4.3(a). Assume that the receiver is at a distance $x$ $(0 < x \leq r)$ from the transmitter. The channel used for this transmission cannot be reused in a circle of radius $r$ around the transmitter and the receiver. Let us denote the area blocked by an omni directional multihop transmission over a distance $x$ as $A_{Omni}(x)$. It is given by the expression $\pi r^2 + \pi r^2 - r^2(q - \sin q)$ where $q = 2 \times \arccos \frac{x}{2r}$. Let $A_{Omni}$ denote the average value of this area. It is given by

$$A_{Omni} = \int_0^r (\frac{2\pi x}{\pi r^2}) A_{Omni}(x) dx \tag{4.3}$$

The area blocked by a directional multihop transmission is shown in Figure 4.3(b) and can be approximated to twice the area of a sector of angle $\theta$ which is equal to $A_{Dir} = r^2\theta$. Note that, we are considering only an approximate estimate of the area blocked by a multihop transmission. Now, the effective area blocked by omni directional and directional multihop transmissions is obtained by taking a weighted average of the values $A_{Omni}$ and $A_{Dir}$ based on the frequency with which a channel is used in omni directional and directional modes. Half the multihop transmissions when the node is in region 1 are omni directional since the BTS uses omni directional transmissions. The remaining half of the transmissions in region 1 and all the transmissions when the node is in region 2 are directional. Thus the average area blocked by a multihop transmission $A_{Blk}$ can be approximated to $\frac{\frac{1}{2}PR(1)A_{Omni}+\frac{1}{2}PR(1)A_{Dir}+PR(2)A_{Dir}}{PR(1)+PR(2)}$. Thus a multihop channel can be reused $\frac{\pi R^2}{A_{Blk}}$ number of times within a cell. Thus the effective number of multihop channels in a cell is given by

$$M = m \times \frac{\pi R^2}{A_{Blk}} \tag{4.4}$$

The remainder of the analysis is similar to the analysis of a TWiLL system. Sections 3.1.4, 3.1.5, 3.1.6 remain unchanged. Analysis in the case when non local calls are made in addition to local calls, the analysis follows along the lines of the analysis of TWiLL described in Section 3.2. We have not incorporated shortcut relaying into our analysis. Thus Section 3.3 does not apply here.

The analysis in the case when propagation models are applied is also similar to the analysis for a TWiLL system given in Sections 3.5, 3.6 and 3.7. Computing the effective radius of multihop transmission is similar to that of TWiLL. After that, the rest of the analysis is similar to that of a simple DWiLL system, as described in this section. The analysis in the cases when log Distance propagation model, Log Normal model and WB model are used thus remains the same.

## 4.2 Simulation Results

To verify the CAR values that were obtained through analysis, we simulated a DWiLL system using GloMoSim [26]. The simulation environment was similar to the one described in Section 3.8.

In the comparison of the analysis and simulation values shown below, it is observed that the values obtained from simulation are always lower than the values obtained from analysis. The reason for this deviation could be that, in the analysis, we have assumed that a multihop channel can be reused as per Equation 4.4 within a cell. But this is not always feasible. Thus the effective number of multihop channels is in reality less than the calculated value and thus the analysis values act as a theoretical upper bound for the simulation values. And hence, the simulation values will always be lower than the analysis values.

We have also computed the CAR values for a traditional WiLL system under similar conditions, both from simulation and from analysis (using Equation 3.14).

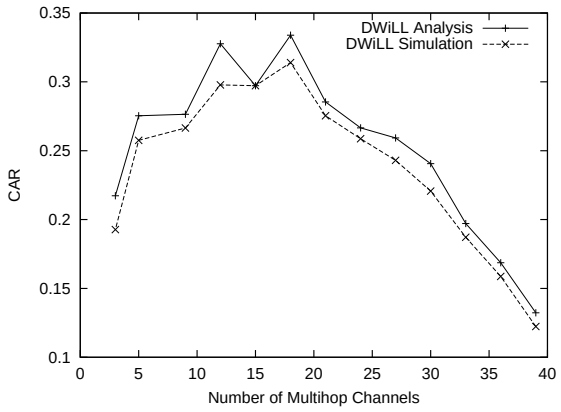


Figure 4.4: Call Acceptance Ratio vs Number of Multihop Channels

These values have been included along with the values of a DWiLL system to illustrate the throughput enhancement achieved by the DWiLL architecture.

### 4.2.1 Call Acceptance Ratio vs Number of Multihop Channels

The number of channels that are required to operate in the multihop mode is in fact a dynamic parameter that a BTS has to decide by taking into consideration the factors such as node density, offered load, the directionality of relaying, and locality of the calls. The number of multihop channels were varied from 3 to 39 and the effect on CAR was observed. As the number of multihop channels increase, call acceptance increases on one hand (as multihop channels are reused unlike single hop channels) and reduces on the other (as single hop channels which are used for downlink are unavailable). Thus there is a trade off involved and it can be found that when the 42 data channels are divided into 18 multihop and 24 single hop channels, the CAR is the highest, as seen in Figure 4.4. This optimum mix of multihop and single hop channels was used for the rest of the simulations.

### 4.2.2 Call Acceptance Ratio vs $\theta$

The azimuth angle of relaying $\theta$ is a significant parameter in the DWiLL system, as it affects the network connectivity, and hence the relative usage of the different types of channels. For a given DWiLL system, we expect $\theta$ to be a fixed parameter. This value was varied over the simulation and the resulting call acceptance was observed. The results are as shown in Figure 4.5. We observe that, as the value of $\theta$ increases, call acceptance increases on one hand (since the probability of finding multihop paths increases) and reduces on the other (since larger area is blocked by a multihop transmission). The CAR was found to be maximum at the value of $\theta = 20°$. This optimum value of $\theta$ obtained from this simulation was used in the rest of the simulations.

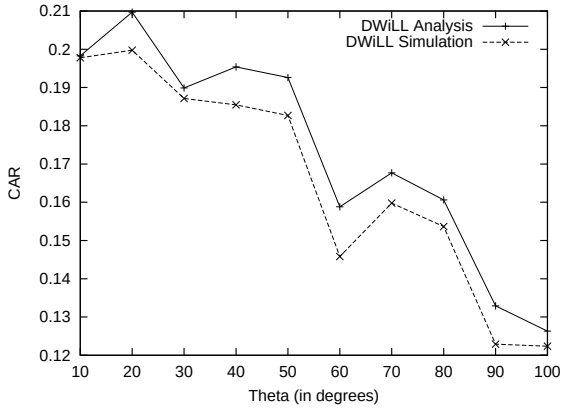


Figure 4.5: Call Acceptance Ratio vs $\theta$

### 4.2.3 Call Acceptance Ratio vs Mean Call Holding Time

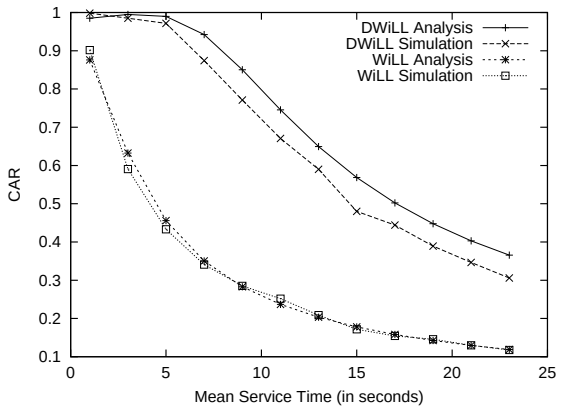


Figure 4.6: Call Acceptance Ratio vs Mean Call Holding Time

In this simulation, the load on the DWiLL system was varied by varying the mean call holding time (or the mean service time of the calls) from a minimum of 1 second to a maximum of 23 seconds. A comparison of the analysis and simulation values is as shown in Figure 4.6. We note that the analysis values are slightly higher than the simulation values, since we have observed earlier that the analysis values are only an upper bound. We also note that a DWiLL system gives a higher throughput than a traditional WiLL system under similar conditions.

### 4.2.4 Call Acceptance Ratio vs Mean Inter Call Arrival Time

The load on the DWiLL system was varied by varying the inter call arrival time of a node. The duration between calls was varied from 22 seconds to 40 seconds. The

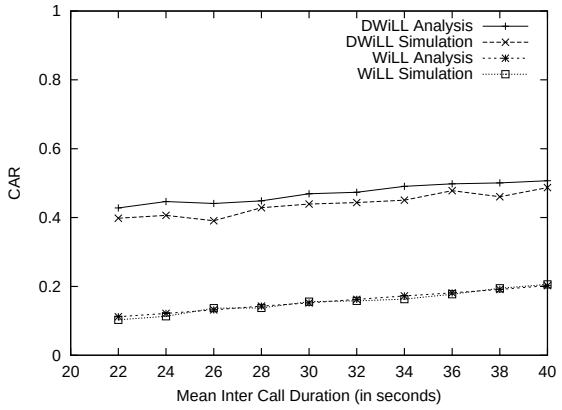


Figure 4.7: Call Acceptance Ratio vs Mean Inter Call Arrival Time

mean call holding time was fixed at 19 seconds. A comparison of the analysis and simulation values is as shown in the Figure 4.7. The CAR increases as the mean duration between calls increases, which is the expected trend, since offered traffic decreases with increasing call arrival rate. The call acceptance values are also lower for a WiLL system compared to a DWiLL system since DWiLL reuses bandwidth.

### 4.2.5 Call Acceptance Ratio vs Node Density

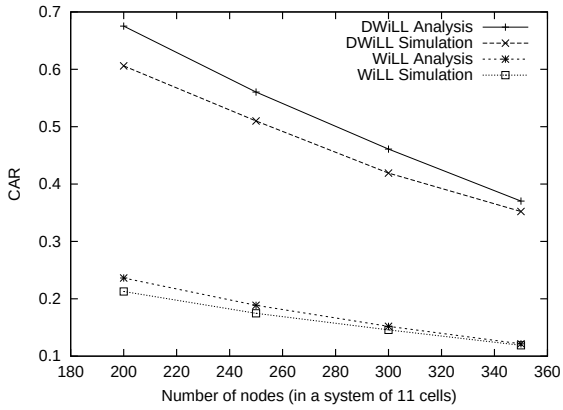


Figure 4.8: Call Acceptance Ratio vs Node Density

The simulations were run with different node densities and the effect on CAR was observed. As the node density increases, the number of calls made in the cell and thus the traffic in the cell increase. A comparison of the analysis and simulation values is as shown in the Figure 4.8. It can be observed that the CAR decreases with increasing node density which is the expected trend.

### 4.2.6 Call Acceptance Ratio vs Locality

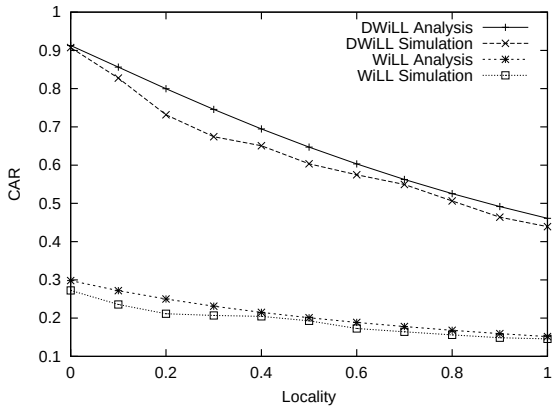


Figure 4.9: Call Acceptance Ratio vs Locality

The locality of the calls was varied from 0 to 1 on a DWiLL system that did not support shortcut relaying. Non local calls were assumed to be terminating outside the WiLL system. When shortcut relaying is not supported, local calls consume more number of channels than non local calls (since, for a non local call, only the source uplink and source downlink calls need to be setup whereas, for a local call, even the destination uplink and destination downlink calls should be setup). Thus, as locality increases, the number of local calls increase and thus the CAR decreases (as shown in Figure 4.9). We also observe the improvement in performance of a DWiLL system when compared to a traditional WiLL system.

### 4.2.7 Call Acceptance Ratio vs Path Loss exponent

Appropriate changes corresponding to the log distance model were made in the radio layer of GloMoSim and the simulations were run. As explained earlier, the coverage area of nodes over single hop channels was maintained at the original value of $R$ by increasing the transmission power in accordance with the path loss exponent. However, the transmission power over multihop channels was not changed with the path loss exponent. Thus the effect of the path loss exponent can be observed. The effect of the path loss exponent $n$ was observed over the following variables: CAR, average hop length and the cardinality of Set B. We recall that Set B is set of nodes which are isolated in the multihop connectivity graph. The value of $n$ was varied from 2 to 6 and the simulation and analysis results were compared.

It can be observed from Figure 4.10 that the CAR reduces with increasing $n$. As the value of $n$ increases, the effective multihop radius reduces. Thus, the average path length increases, as seen in Figure 4.11. This necessitates the use of more multihop channels. Though this is offset to a certain extent by increased reuse of multihop channels (since, now a multihop transmission effectively blocks lesser area), the CAR

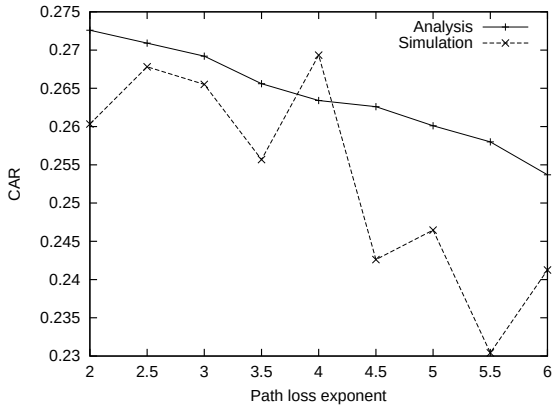


Figure 4.10: Call Acceptance Ratio vs Path Loss exponent

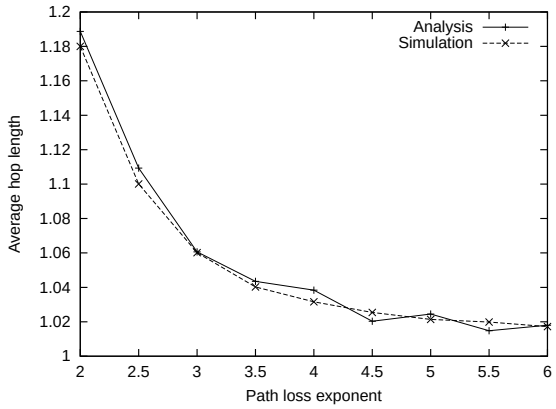


Figure 4.11: Average Hop Length Vs Path Loss exponent

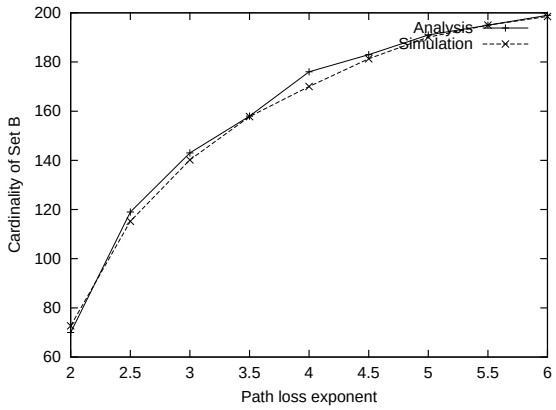


Figure 4.12: Cardinality of Set B Vs Path Loss exponent

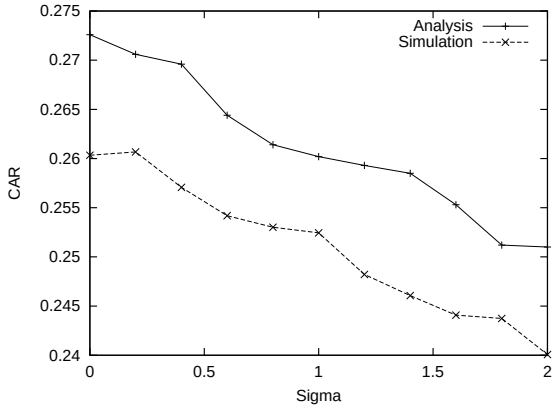


Figure 4.13: Call Acceptance Ratio vs Sigma - Unrestricted case

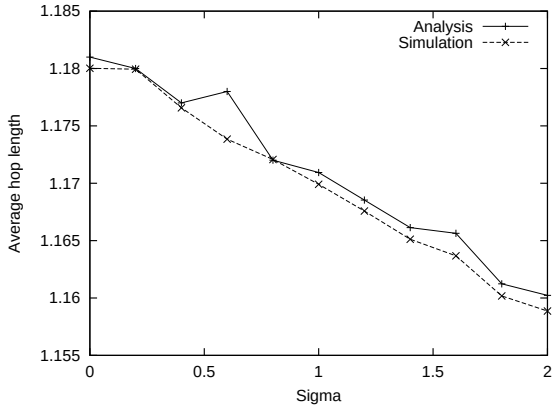


Figure 4.14: Average Hop Length vs Sigma - Unrestricted case

still reduces. This can also be explained by the increase in the cardinality of Set B, as seen in Figure 4.12 which reduces multihop connectivity and thus the formation of multihop paths. One important observation is that the effect of the path loss exponent is more pronounced in TWiLL than in DWiLL. The fact that the usage of multihop channels was more in TWiLL than in DWiLL, coupled with our assumption that only multihop transmissions are effected by the propagation models, justifies this observation.

### 4.2.8 Call Acceptance Ratio vs Sigma

The changes corresponding to the log normal model were incorporated into the radio layer of GloMoSim and the simulations were run. The value of $\sigma$ was varied between 0 and 2 and the effect on CAR and average hop length was observed.

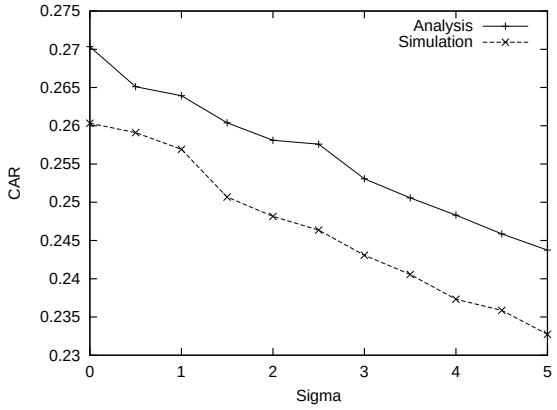


Figure 4.15: Call Acceptance Ratio vs Sigma - Restricted case

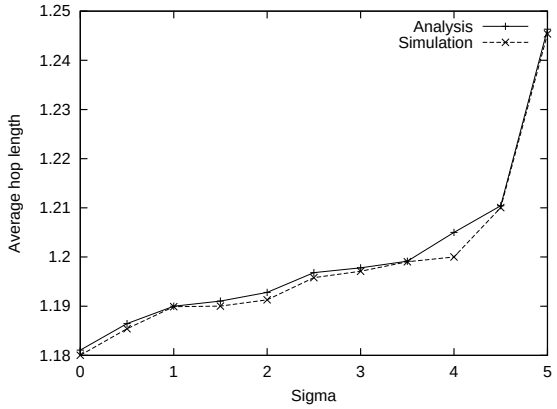


Figure 4.16: Average Hop Length vs Sigma - Restricted case

In the unrestricted case, it can be observed from Figure 4.13 that the CAR decreases with increasing $\sigma$, which is justified since shadowing effects hinder multihop connectivity. Also, the effective radius increases with increasing $\sigma$, which can be deduced from the decreasing hop length, as shown in Figure 4.14.

In the restricted case, it can be observed from Figure 4.15 that the CAR decreases with increasing $\sigma$, which is justified since shadowing effects hinder multihop connectivity. Also, the effective radius decreases with increasing $\sigma$, which can be deduced from the increasing hop length, as shown in Figure 4.16. Note that the effect of $\sigma$ is more pronounced in the case of the restricted case than in the unrestricted case, which is justified since the coverage area is effected more in the restricted case. Also, the effect of $\sigma$ is more pronounced in TWiLL than in DWiLL since the dependence on multihop channels is more in TWiLL.

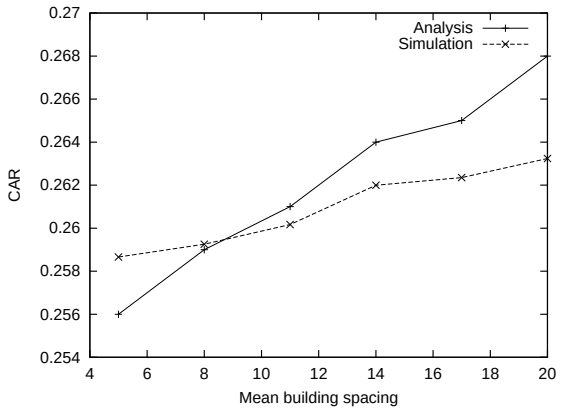


Figure 4.17: Call Acceptance Ratio vs Mean spacing between buildings

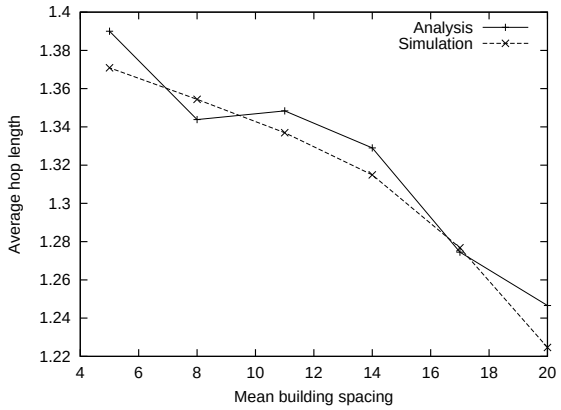


Figure 4.18: Average Hop Length vs Mean spacing between buildings

### 4.2.9 Call Acceptance Ratio vs Terrain Parameters in WB model

The changes corresponding to the WB model were incorporated into the radio layer of GloMoSim and the simulations were run. The mean separation between buildings was varied by changing the parameter $\frac{d}{\lambda}$ between 5 and 20. The mean height of the buildings was also varied by changing the parameter $\delta h_b$ between 50 and 100.

It can be observed from Figure 4.17 that the CAR increases with increasing $\frac{d}{\lambda}$, which is justified since closely packed buildings tend to cause more diffraction effects. Also, the effective radius increases with increasing $\frac{d}{\lambda}$, which can be deduced from the decreasing hop length, as shown in Figure 4.18.

It can be observed from Figure 4.19 that the CAR increases with increasing $\delta h_b$, which is justified since larger height difference between the BTS and the buildings causes lesser diffraction. Also, the effective radius increases with increasing $\delta h_b$, which can be deduced from the decreasing hop length, as shown in Figure 4.20.

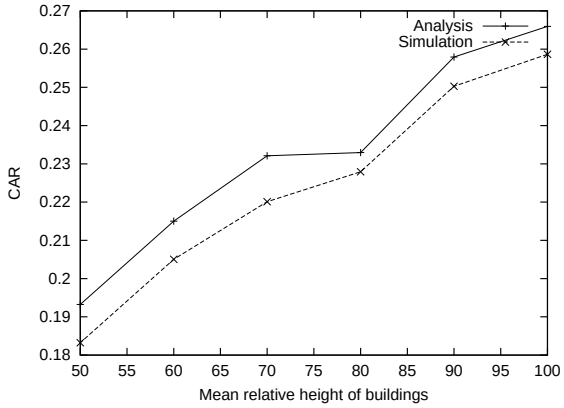


Figure 4.19: Call Acceptance Ratio vs Relative height of buildings

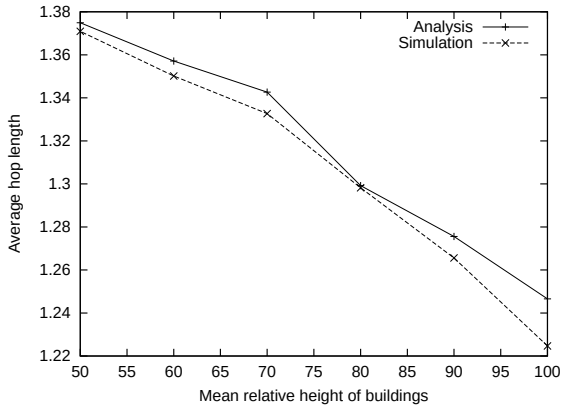


Figure 4.20: Call Acceptance Ratio vs Relative height of buildings

# CHAPTER 5

# Conclusions and Future Work

Bandwidth is a scarce commodity in WiLL systems, as is the case with any wireless system, and multihop relaying is a powerful technique in helping us reuse this scarce resource. Through the course of this work, we have observed that directional multihop relaying leads to significant bandwidth reuse in the WiLL architecture and hence the TWiLL and DWiLL systems perform consistently better than the traditional WiLL systems. They are also more robust at high loads. Techniques like shortcut relaying further improve the performance of multihop relaying systems, especially in systems with high locality. Directional transmissions have other added advantages like low power consumption and lesser probability of detection. We have observed that TWiLL and DWiLL systems, on an average, provide a performance improvement of upto 10% at light load, upto 150% at moderate load and upto 60% at very high load.

Having realized the inadequacies of traditional formulas like the Erlang B Loss formula in predicting the performance of multihop networks, we have come up with a fairly accurate theoretical modeling of multihop WiLL architectures using multi dimensional Markov chains. We have corroborated our analysis with experimental values from simulations and thus verified the correctness of our model. We have evaluated the performance of TWiLL and DWiLL under different loads, node densities and localities using our mathematical model and using simulations.

We have also identified some realistic propagation models and studied the performance of TWiLL and DWiLL systems with these models. We have incorporated the log distance path loss model, the log normal path loss model and the Walfisch Bertoni model into our analysis and simulation.

Some pointers for future research related to this work are:

- In the DWiLL architecture, the channel allocation scheme we used was a naive one, where we serially examined all the channels that were allocated to a cell and chose the first one that did not interfere with any ongoing transmission. A more optimum channel allocation scheme can be devised and used.
- In our work, we have assumed that the number of multihop channels, single hop channels and parameters like $r$ and $\theta$ are all fixed. However, they can be dynamic parameters being controlled by the BTS based on the current load of the system.
- In the TWiLL and DWiLL architectures, we have assumed that single hop channels are used by a node only when no multihop path is available i.e., when

a node is isolated. A node does not use a single hop channel if a multihop path exists but multihop channel allocation fails. This provision can be made in the future revisions.

- While incorporating propagation models into the analysis, we have assumed that the BTS regulates its transmission power on the control channel in such a way that shadowing effects do not in any way hinder the delivery of control messages, which are important to ensure correct topology building. This assumption can be relaxed.
- We have considered only a simplified version of the WB propagation model, where the receiver antenna is mounted over the rooftop and is of negligible height when compared to the height of the building. These assumptions can be relaxed by extending the analysis.
- We have considered only a few of the myriad propagation models present. More models can be examined.

# Bibliography


[**1**] Peter Stavroulakis (Editor), Wireless Local Loops, Theory and Applications, Wiley, June 2001.

[**2**] H. Ochsner, "DECT Digital European Cordless Telecommunications", in *Proceedings of IEEE Vehicular Technology 39th Conference*, pp. 718-721, May 1989.

[**3**] D. C. Cox, W. Arnold, and P. T. Porter, "Universal Digital Portable Communications: A System Perspective", in *IEEE Journal on Selected Areas in Communications*, Vol. 5, No. 5, pp. 764-773, June 1987.

[**4**] K. Ogawa, et. al., "Toward the Personal Communication Era the Radio Access Concept from Japan", in *International Journal on Wireless Information Networks*, Vol. 1, No. 1, pp. 17-27, January 1994.

[**5**] H. Wu, C. Qiao, S. De, and O. Tonguz, "Integrated Cellular and Ad Hoc Relaying Systems: iCAR," in *IEEE Journal on Selected Areas in Communications*, Vol. 19, No. 10, pp. 2105-2115, October 2001.

[**6**] H. Wu and C. Qiao, "Modeling iCAR via Multi-dimensional Markov Chains", in *ACM Mobile Networking and Applications (MONET), Special Issue on Performance Evaluation of Qos Architectures in Mobile Networks*, Vol. 8, no. 3, pp. 295-306, 2003.

[**7**] H. Y. Hsieh and R. Sivakumar, "Performance Comparison of Cellular and Multihop Wireless Networks: A Quantitative Study," in *Proceedings of ACM SIGMETRICS 2001*, pp. 113-122, Cambridge, MA, USA, June 2001.

[**8**] Y. D. Lin and Y. C. Hsu, "Multihop Cellular: A New Architecture for Wireless Communications," in *Proceedings of IEEE INFOCOM 2000*, Vol. 3, pp. 1273-1282, March 2000.

[**9**] R Ananthapadmanabha, B. S. Manoj, and C. Siva Ram Murthy, "Multihop Cellular Networks: The Architecture and Routing Protocols", in *Proceedings of IEEE PIMRC 2001*, pp. 573-576, October 2001.

[**10**] B. S. Manoj, Christo Frank. D, and C. Siva Ram Murthy "Throughput Enhanced Wireless in Local Loop (TWiLL) - The Architecture, Protocols and Pricing Schemes", in *ACM Mobile Computing and Communications Review*, Vol. 7, No. 1, pp. 95-116, January 2003.

[**11**] C. Lau and C. Leung,"A Slotted ALOHA Packet Radio Networks with Multiple Antennas and Receivers", in *IEEE Transactions on Vehicular Technology*, Vol. 39, No. 3, pp. 218-226, March 1990.

[**12**] N. Pronios, "Performance Considerations for Slotted Spread Spectrum Random Access Networks with Directional Antennas", in *Proceedings of IEEE GLOBECOM '89*, Vol. 3, pp. 1613-1617, November 1989.

[**13**] T. S. Yum and K. W. Hung, "Design Algorithms for Multihop Packet Radio Networks with Multiple Directional Antenna Stations", in *IEEE Transactions on Communications*, Vol. 40, No. 11, pp. 1716-1724, November 1992.

[**14**] Y. B. Ko, V. Shankarkumar, and N. H. Vaidya, "Medium Access Control Protocols Using Directional Antennas in Ad Hoc Networks" in *Proceedings of IEEE INFOCOM '00*, Vol. 1, pp. 13-21, March 2000.

[**15**] A. Spyropoulos and C. S. Raghavendra, "Energy Efficient Communications in Ad Hoc Networks Using Directional Antennas", in *Proceedings of IEEE INFOCOM' 02*, Vol. 1, pp. 220-228, June 2002.

[**16**] T. S. Rappaport, Wireless Communications: Principles and Practice, Prentice Hall, 1996.

[**17**] D. Har, H. H. Xia and H. L. Bertoni, "Path Loss Prediction Model for Microcells", in *IEEE Transactions on Vehicular Technology*, Vol. 48, Issue 5, pp. 1453-1462, September 1999.

[**18**] J. Walfisch, and H. L. Bertoni, "A Theoritical Model of UHF Propagation in Urban Environments", in *IEEE transactions on Antennas and Propagation*, Vol. 124, No. 2, pp. 95-102, December 1977.

[**19**] H. H. Xia, and H. L. Bertoni, "Diffraction of Cylindrical and Plane waves by an Array of Absorbing Half Screens", in *IEEE Transactions on Antennas and Propagation*, Vol. 40, No. 2, pp. 170-177, February 1992.

[**20**] L. E. Vogler, "An Attenuation function for Multiple Knife Edge Diffraction", in *Radio Science*, Vol. 17, No. 3, pp. 1541-1546, May 1982.

[**21**] S. R. Saunders, and F. R. Bonar, "Prediction of Mobile Radio Wave Propagation over Buildings of Irregular Heights and Spacing", in *IEEE Transactions on Antennas and Propagation*, Vol. 42, No. 2, pp. 137-144, February 1994.

[**22**] J. B. Anderson, "UTD Multiple Edge Transition Zone Diffraction", in *IEEE Transactions on Antennas and Propagation*, Vol 45, No. 2, pp. 1093-1097, February 1997.

[**23**] Dimitri P. Bertsekas, Robert Gallager, Data Networks, 2nd Edition, Prentice-Hall, 1992.

[**24**] G. R. Cooper, and C. D. McGillem, Probabilistic Methods of Signal and System Analysis, Holt, Rinehart, and Winston, New York, 1986.

[**25**] J. M. Holtzman, "A Simple, Accurate Method to Calculate Spread Spectrum Multiple Access Error Probabilities", in *IEEE Transactions on Communications*, Vol. 40, No. 3, pp. 461-464, March 1992.

[**26**] GloMoSim: A Library for Parallel Simulation of Large-scale Wireless Networks, in *Proceedings of PADS-98, Banff, Canada*, May 1998.

[**27**] V. Mythili Ranganath, B. S. Manoj, C. Siva Ram Murthy, "Performance Evaluation of Multihop Wireless in Local Loop Architectures", Technical Report, HPCN Lab, Department of Computer Science and Engineering, IIT Madras, May 2004.